

(NASA-TM-105495) DIRECT SIMULATION MONTE
CARLO WITH IONIZATION AND RADIATION Ph.D.
Thesis, North Carolina State Univ. (NASA)
82 p CSCL 20N

N92-25455

Unclas
G3/32 0091387

DIRECT SIMULATION MONTE CARLO WITH IONIZATION AND RADIATION

by

Ann B. Carlson

A thesis submitted to the Graduate Faculty of
North Carolina State University
in partial fulfillment of the
requirements for the Degree of
Doctor of Philosophy

Department of Mechanical and Aerospace Engineering

Raleigh

1990

LIBRARY COPY

JAN 30 1991

LANGLEY RESEARCH CENTER
LIBRARY NASA
HAMPTON, VIRGINIA

91387

DIRECT SIMULATION MONTE CARLO WITH IONIZATION AND RADIATION

by

Ann B. Carlson

A thesis submitted to the Graduate Faculty of
North Carolina State University
in partial fulfillment of the
requirements for the Degree of
Doctor of Philosophy

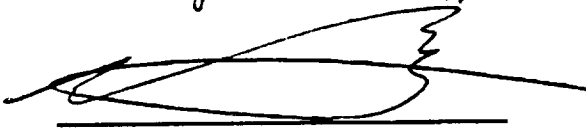
Department of Mechanical and Aerospace Engineering

Raleigh

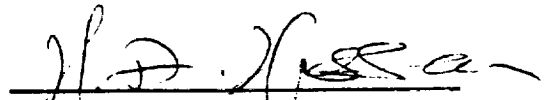
1990

Approved By:

Wayland C. Kuyfitt



Ernest R. Dejanette



Chairman of Advisory Committee

ABSTRACT

Carlson, Ann B. Direct Simulation Monte Carlo with Ionization and Radiation (Under the direction of Dr. H. A. Hassan)

Improvements in the modeling of radiation in low density shock waves with Direct Simulation Monte Carlo (DSMC) are the subject of this study. The physical processes which determine the amount of radiation in a shock wave were investigated and the way in which they are modeled with DSMC were evaluated. Three physical processes were identified for which an improvement in the modeling technique could result in improved radiation predictions. New physical modeling schemes are introduced in this report for the three processes. First a method for determining the electric field and its effect on the flow is introduced. The electric field is obtained by satisfying the requirements of ambipolar diffusion in the flow. Second, a two step reaction process for electron impact ionization reactions is evaluated. Finally, a new scheme to determine the relaxation collision numbers for excitation of electronic states is proposed. Each new scheme attempts to move the DSMC method toward more accurate physics or more reliance on available experimental data. The new schemes are all compared to the current modeling techniques and the differences in the results are evaluated. The new modeling schemes do not introduce any significant computational time penalties. The test case, for which some AVCO-Everett shock tube data exist, is a 10 km/s standing shock wave in air at .1 Torr. In all cases the results agree with the available data as well as, or better than the results from the earlier schemes.

ACKNOWLEDGEMENTS

It is commonly said in graduate student circles that *a professor is someone who speaks in someone else's sleep*. This could certainly be said of a good research advisor; for without the constant communication, advice, and gentle prodding few graduate research projects would ever be completed. With this in mind, I would like to thank Professor H. A. Hassan, the chairman of my advisory committee, for his continued guidance and encouragement. The other members of my advisory committee also deserve thanks for their assistance and helpfulness.

In addition to my faculty committee, several other researchers have been of valuable assistance to me in performing this work. The personnel in the Aerothermodynamics and Engineering Analysis Branches at NASA Langley Research Center have been very supportive, particularly Dr. James N. Moss, Ms. Lin C. Hartung and Mr. Chris J. Riley. I would also like to express my appreciation to Professor G. A. Bird for his advice and continuing interest.

Finally, I must acknowledge the contributions of my husband and family to the completion of this research. Without their continued flexibility and emotional support I would not have gotten this far.

TABLE OF CONTENTS

LIST OF FIGURES	v
LIST OF TABLES	vii
1 INTRODUCTION	1
2 THE DSMC METHOD	6
2.1 DSMC	6
2.2 Real Gas Collisions	8
2.3 Chemical Reactions	10
2.4 Thermal Radiation	14
3 THE TEST CASE	22
3.1 The AVCO Experiment	22
3.2 The 1-D DSMC Code	23
4 MODELING OF PLASMAS	25
4.1 The Method of Bird	27
4.2 The Ambipolar Diffusion Method	29
4.3 Results	31
5 ELECTRON IMPACT IONIZATION	37

	iv
5.1 One Step Method	37
5.2 The Two Step Method	39
5.3 Results	41
6 RADIATION CALCULATIONS	43
6.1 The Qualitative Approach	43
6.2 The Proposed Method	45
6.3 Results	48
6.3.1 Nonequilibrium Radiation	52
6.3.2 Equilibrium Radiation	56
7 CONCLUDING REMARKS	59
REFERENCES	62
8 APPENDIX A: ELECTRIC FIELD CALCULATIONS	65
9 APPENDIX B: RELAXATION NUMBERS	67

LIST OF FIGURES

1.1	Analysing the transitional flow regime	1
4.1	Composition through the shock	32
4.2	Translational temperature through the shock	33
4.3	Electron temperature through the shock	34
4.4	Electric field through the shock	35
4.5	Electron concentration through the shock	35
4.6	Global radiation through the shock	36
5.1	Electron temperature through the shock	42
5.2	Electron concentration through the shock	42
6.1	Global radiation through shock	49
6.2	Oscillogram trace of radiation from AVCO experiment	50
6.3	Translational temperature through the shock	51
6.4	Electron temperature through the shock	51
6.5	Radiation intensity vs. wavelength, Bird's method	53
6.6	Radiation intensity vs. wavelength, new method	53
6.7	Molecular contributions to total radiation	54
6.8	Contribution of atomic nitrogen to total radiation	54
6.9	Contribution of atomic oxygen to total radiation	55

6.10 Radiation intensity vs. wavelength, Bird's method	56
6.11 Radiation intensity vs. wavelength, new method	57
6.12 Molecular contributions to total radiation	57
6.13 Contribution of atomic nitrogen to total radiation	58
6.14 Contribution of atomic oxygen to total radiation	58

LIST OF TABLES

2.1	VHS molecular diameters at 288K	10
2.2	List of Chemical Reactions	13
2.3	Electronic states for O_2	16
2.4	Electronic states for N_2	17
2.5	Electronic states for N_2^+	18
2.6	Electronic states for NO	18
2.7	Molecular band system	19
2.8	Groups of electronic states for O	19
2.9	Groups of states for N	20
2.10	Radiative transitions for O	20
2.11	Radiative transitions for N	21
6.1	Relaxation collision numbers for electronic excitation	44
6.2	Relaxation collision numbers for electronic excitation	47
9.1	Excitation rate coefficients from NEQAIR	68
9.2	Rate coefficients for N_2 , fifth level	72
9.3	Rate coefficients for O_2	73

1 INTRODUCTION

The recent interest in planetary aerobraking vehicles or aeroassisted orbital transfer vehicles has led to the need to perform analyses in the transitional flow regime. At altitudes below the range for free molecule calculations but above the applicability of continuum calculations, the Monte Carlo calculation techniques are appropriate (see Figure 1.1). The Direct Simulation Monte Carlo (DSMC) technique of Bird[1] is the computational technique used in this study of hypersonic shock flow in the transitional regime.

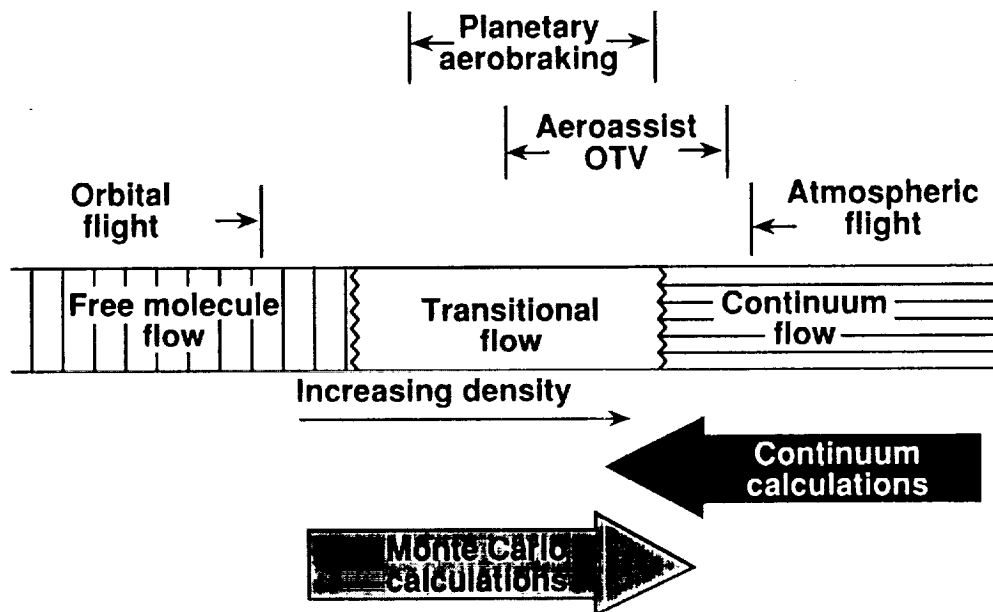


Figure 1.1. Analyzing the transitional flow regime

The DSMC method involves the physical simulation of gas particles in a flowfield

as they undergo collisions, boundary interactions and chemical reactions. The success of this method has been in its ability to model highly nonequilibrium flows such as are encountered in reentry shock waves.

At reentry velocities in the upper atmosphere, radiation from the shock wave can be a significant portion of the overall heat transfer to the vehicle. Accurate predictions of this radiation in nonequilibrium shocks is required for efficient design of thermal protection systems. Although the ability to model the process of radiation with DSMC has been demonstrated by Bird[2] and Moss[3], much of the current modeling is very approximate. Verification of the modeling techniques and investigations of alternate techniques are required to improve the level of confidence in the radiation predictions. The present study addresses this goal through investigating the modeling of the electric field, electron impact ionization, and collisional electronic excitation.

Because the most efficient excitation of the electronic states involved with radiation is through collisions with electrons or ions, the correct modeling of ionization is essential. Along with the correct modeling of the ionization reactions, the effect of the electric field must be considered in flows involving significant levels of ionization. Early DSMC simulations allowed only a crude approximation to the electric field. Each ion was associated with an electron and this pair was always moved together. An electric field based on a continuum equation was determined from the converged solution for electron density gradient and temperature. This field would then be introduced into the simulation and a new solution obtained. The process would be

repeated until the changes between successive iterations were sufficiently small. A new method of handling the electric field has been proposed which involves using the concept of ambipolar diffusion to determine a cell electric field. This method has the advantage of fitting within the DSMC framework and incorporating the full range of flow gradients into the determination of the electric field.

While the data used in DSMC simulations for most of the chemical reactions are considered to be good, the modeling of electron impact ionization reactions has involved an approximation that can significantly impact the prediction of ionization. DSMC uses the ratio of the reaction cross-section to the collision cross-section to determine the probability of a reaction. Because reaction cross-sections are not generally available in the literature, one is calculated from the Arrhenius form of a rate equation each time a reaction occurs. The available rate data for electron impact ionization reactions contain large, negative exponents on the temperature term. These highly negative temperature exponents cause problems when incorporating these equations into the usual DSMC procedure. When the temperature dependent rate coefficients are converted to collisional energy dependent steric factors, a limit on the exponent is obtained which does not allow the reaction rate to be used in the form which best fits the data. One technique is to evaluate the reaction rate at an average temperature for the flow and use the non-temperature dependent form of the coefficient in the simulation. A new method has been proposed which treats electron impact ionization reactions as a two step process, an idea which has gained increasing theoretical

and experimental backing in recent years. If the reaction is treated as proceeding in two steps, the DSMC formulation for collisional energy dependent steric factors can be used without sacrificing any of the experimentally determined temperature dependence.

The thermal radiation due to bound-bound transitions between electronic states appears to dominate over other forms of radiation for velocities in excess of 9 km/s[4]. One of the main difficulties with modeling this radiation is determining the collisional excitation rates for the various excited states. The method uses a collision number which represents the fraction of collisions between certain species which lead to excitation of electronic states for one or both of the particles. Because of the incompleteness of data available on excitation cross-sections, these numbers were, at first[2], chosen based on a qualitative knowledge of the magnitudes of the various cross-sections. They were further refined to match available data from appropriate temperature regimes. A new method has been developed which bases these numbers on the available excitation rate data. The equation for the production of a species is related to a characteristic time which is, in turn, used to determine a collision number through comparison with the collision frequency. While any method will remain quite approximate until better data are available on excitation cross-sections and rates, this method has the advantage of incorporating all of the species density and temperature dependence into the calculation of collision number. It should, therefore, be valid over a wider range of temperature and flowfield conditions.

A sample problem of a 10 km/s shock wave in air at .1 Torr has been used to evaluate the newly developed methods. This test case was chosen because it represents the conditions of a shock tube investigation of nonequilibrium radiation which was performed at AVCO-Everett Research Laboratory in the early 1960's[4]. The calculations are performed with a one-dimensional standing shock wave DSMC program. Differences between the methods are evaluated. Wherever possible, the results are compared with measurements from the AVCO experiment.

2 THE DSMC METHOD

This computational method was developed primarily by Professor Graeme Bird, formerly of the University of Sydney, Australia. There are many different physical models of processes used in various DSMC schemes. The following discussion covers the main aspects of the form of the method which has been used in this work.

2.1 DSMC

The Direct Simulation Monte Carlo (DSMC) method uses a direct physical simulation approach to solving the flow of low density gases. Because the molecular structure of a gas at low densities must be accounted for in the solution process, the problem lends itself to direct physical description. The gas is modeled by thousands of simulated molecules in a computer. The position, velocity and internal state of each molecule are stored in the computer and modified as the molecule undergoes collisions and boundary interactions. While all the collisions are treated as fully three-dimensional, advantage may be taken of flow symmetries to reduce the number of parameters which must be stored for each molecule. For example, in a one-dimensional flow only the position coordinate in the direction of flow gradients would be stored. All procedures may be specified such that the computation time is linearly dependent on the number of molecules. With today's high speed computers, the solution of real engineering problems is practical and is becoming routine even in two and three dimensions.

The flow is always unsteady and the time parameter in the simulation may be identified with real time. The time parameter is advanced according to the collision frequency appropriate to the flow. A critical assumption in the DSMC method is that the molecular motion and intermolecular collisions may be uncoupled over the small time step, Δt , used to advance the calculation. Thus, collisions between the particles proceed until the time is advanced by Δt , then the particles are moved a distance appropriate to their velocities and Δt . This has been shown[5] to be valid when the time step is less than the local average collision time

$$\Delta t < 1/\nu \quad (2.1)$$

where ν is the local average collision frequency. Particles enter or exit the flow at computational boundaries representing a free stream, vacuum or a known flow solution. Boundary conditions may be such that a steady flow is obtained as the large time state of the unsteady flow.

A computational cell is required for the selection of collision partners and for sampling the macroscopic quantities in the flow. The cell dimension must be small in comparison with the scale length of any macroscopic flow gradients. In regions with large gradients, such as a shock wave, the cell dimension must be a fraction of the mean free path to meet this criterion. Typically the cell dimension, Δr , is chosen as

$$\Delta r < \lambda/3 \quad (2.2)$$

where λ is the local mean free path. Flow properties are determined from the averages of particle properties in a cell taken over a very large number of samples.

2.2 Real Gas Collisions

Collisions between molecules proceed based on a knowledge of the collision cross-section. If more theoretical and experimental information on collision cross-sections were available, the exact values could be used in the simulation. However, at the moment the cross-sections must be calculated from an assumed molecular interaction model. The Variable Hard Sphere (VHS) model is used. This model has been shown[5] to be the simplest model which provides sufficient accuracy to model real gas flows which contain diatomic molecules.

The VHS model combines features of the hard sphere molecules with molecules interacting according to an inverse power law. Thus, the model has a well defined diameter which is an inverse power law function of the relative collisional energy between the colliding molecules. As a result, the total cross-section, σ_T , can be expressed as

$$\sigma_T = \pi d^2 \propto (1/2 m_r C_r^2)^{-\omega} \quad (2.3)$$

where d is the reference diameter, m_r is the reduced mass, and C_r is the relative velocity. For an inverse power law model the force, F , behaves as

$$F \propto 1/r^\eta \quad (2.4)$$

where r is the intermolecular separation. In this case

$$\sigma_T \propto C_r^{-4/(\eta-1)}. \quad (2.5)$$

A comparison of the two equations for σ_T gives

$$\omega = 2/(\eta - 1) \quad (2.6)$$

The appropriate value of η or ω for a given simulation is deduced from the viscosity law which, for an inverse power law, yields viscosity, μ , as

$$\mu \propto T^{\omega+1/2}. \quad (2.7)$$

The model that is used for the partitioning of internal energy requires a common viscosity-temperature dependence for all molecular species. The value of ω was assumed to be 0.2 and the molecular diameters at the reference temperature of 288 K are given in Table 2.1. The effective elastic diameter of the electrons is the most uncertain but it is generally assumed to be less than that of the atoms and molecules. An earlier study[6] found the DSMC results to be not greatly sensitive to changes in the choice of electron diameter.

The phenomenological model introduced by Borgnakke and Larsen[7] is used for the internal energy calculations. The main feature of this model is that a fraction of the collisions are regarded as completely inelastic. For these, new values of internal energies are sampled from the distributions of these quantities that are appropriate to an equilibrium gas. The number of degrees of freedom in the partially excited vibrational states is calculated from harmonic oscillator theory. The remainder of molecular collisions are treated as completely elastic. The fraction of inelastic collisions is chosen to approximately match the real gas relaxation rates. These rates

Table 2.1. VHS molecular diameters at 288 K

Species	Diameter ($\text{m} \times 10^{10}$)
O_2, O_2^+	3.96
N_2, N_2^+	4.07
O, O^+	3.
N, N^+	3.
NO, NO^+	4.
e^-	1.

are a function of temperature but, because of the lack of precise data at appropriate temperatures, constant collision numbers of 5 and 50 were used for the rotational and vibrational modes, respectively.

2.3 Chemical Reactions

The procedures for the nonequilibrium chemical reactions are extensions of the elementary collision theory of chemical physics. The binary reaction rate is obtained as the product of the collision rate for collisions with energy in excess of the activation energy and the probability of reaction or steric factor. The chemical data for gas phase reactions, quoted in terms of the continuum rate coefficient, $k(T)$, are specified by

$$k(T) = aT^b \exp(-E_a/(kT)) . \quad (2.8)$$

The constants a and b are determined by matching the equations to a set of experimental data over a range of temperatures. A form of the collision theory that is consistent with the VHS model has been used to convert these temperature dependent rate coefficients of continuum theory into collisional energy dependent steric factors. The steric factor, P_r , which is the ratio of the reaction cross-section to the total cross-section that results in the above rate coefficient is proportional to

$$P_r \propto (1 - E_a/E_c)^{\zeta+b+1/2}, \quad E_c \geq E_a$$

$$P_r = 0, \quad E_c < E_a \quad (2.9)$$

where ζ , the effective number of internal degrees of freedom, is given by $\zeta = (\zeta_1 + \zeta_2)/2$, with subscripts 1 and 2 referring to the colliding molecules. For diatomic molecules, ζ is usually less than four. With P_r equal to zero for collisional energy less than activation energy ($E_c < E_a$), a representation similar to that given by Equation 2.8 is valid as long as

$$\zeta + b + 1/2 > 0. \quad (2.10)$$

A total of 41 chemical reactions are included in the modeling. The reaction rates are based on the set proposed by Park and Menees[8]. The reaction rate coefficients are given in Table 2.2.

The temperature variation for some reactions involving charged particles is such that the criterion of equation 2.10 is not met. For example, values of b for the reactions



and



given by Park and Menees are -3.9 and -3.82 respectively. Because the reactants are monatomic molecules, $\zeta = 0$. Thus, b cannot be less than $-1/2$ for the modeling to be valid and the reported reaction rates are not consistent with the steric factor formulation. The method which has been employed is to select an average flow temperature and replace T^b in Equation 2.8 by its value at that temperature. This method adds significantly to the uncertainty in the flowfield ionization prediction. A new method to account for these reactions without sacrificing the temperature dependence will be discussed in a later section.

Table 2.2. List of Chemical Reactions

Number	Reaction (Energy in J)	Rate Coefficient ($\text{m}^3/(\text{molecule s})$) $k(T) = aT^b \exp(-E_a/kT)$
1	$O_2 + N + 8.197 \times 10^{-19} \rightarrow 2O + N$	$1.375 \times 10^{-10} T^{-1} \exp(-59370/T)$
2	$O_2 + NO + 8.197 \times 10^{-19} \rightarrow 2O + NO$	$4.580 \times 10^{-11} T^{-1} \exp(-59370/T)$
3	$O_2 + N_2 + 8.197 \times 10^{-19} \rightarrow 2O + N_2$	$4.580 \times 10^{-11} T^{-1} \exp(-59370/T)$
4	$O_2 + O_2 + 8.197 \times 10^{-19} \rightarrow 2O + O_2$	$4.580 \times 10^{-11} T^{-1} \exp(-59370/T)$
5	$O_2 + O + 8.197 \times 10^{-19} \rightarrow 3O$	$1.375 \times 10^{-10} T^{-1} \exp(-59370/T)$
6	$N_2 + O + 1.561 \times 10^{-18} \rightarrow 2N + O$	$1.850 \times 10^{-8} T^{-1.6} \exp(-113000/T)$
7	$N_2 + O_2 + 1.561 \times 10^{-18} \rightarrow 2N + O_2$	$6.170 \times 10^{-9} T^{-1.6} \exp(-113000/T)$
8	$N_2 + NO + 1.561 \times 10^{-18} \rightarrow 2N + NO$	$6.170 \times 10^{-9} T^{-1.6} \exp(-113000/T)$
9	$N_2 + N_2 + 1.561 \times 10^{-18} \rightarrow 2N + N_2$	$6.170 \times 10^{-9} T^{-1.6} \exp(-113000/T)$
10	$N_2 + N + 1.561 \times 10^{-18} \rightarrow 3N$	$1.850 \times 10^{-8} T^{-1.6} \exp(-113000/T)$
11	$NO + N_2 + 1.043 \times 10^{-18} \rightarrow N + O + N_2$	$3.830 \times 10^{-13} T^{-0.5} \exp(-75550/T)$
12	$NO + O_2 + 1.043 \times 10^{-18} \rightarrow N + O + O_2$	$3.830 \times 10^{-13} T^{-0.5} \exp(-75550/T)$
13	$NO + NO + 1.043 \times 10^{-18} \rightarrow N + O + NO$	$3.830 \times 10^{-13} T^{-0.5} \exp(-75550/T)$
14	$NO + O + 1.043 \times 10^{-18} \rightarrow N + 2O$	$7.660 \times 10^{-13} T^{-0.5} \exp(-75550/T)$
15	$NO + N + 1.043 \times 10^{-18} \rightarrow 2N + O$	$7.660 \times 10^{-13} T^{-0.5} \exp(-75550/T)$
16	$NO + O + 2.190 \times 10^{-19} \rightarrow N + O_2$	$3.600 \times 10^{-22} T^{1.29} \exp(-19700/T)$
17	$N_2 + O + 5.175 \times 10^{-19} \rightarrow N + NO$	$5.300 \times 10^{-17} T^{0.1} \exp(-37500/T)$
18	$O_2 + N \rightarrow 2.190 \times 10^{-19} + O + NO$	$5.200 \times 10^{-22} T^{1.29} \exp(-3600/T)$
19	$NO + N \rightarrow 5.175 \times 10^{-19} + O + N_2$	$2.020 \times 10^{-17} T^{0.1}$
20	$N + O + 4.422 \times 10^{-19} \rightarrow NO^+ + e^-$	$2.550 \times 10^{-20} T^{0.37} \exp(-32030/T)$
21	$O + e^- + 2.180 \times 10^{-18} \rightarrow O^+ + 2e^-$	$3.000 \times 10^{-12} \exp(-157900/T)$
22	$O + O + 1.120 \times 10^{-18} \rightarrow O_2^+ + e^-$	$6.420 \times 10^{-22} T^{0.49} \exp(-81100/T)$
23	$O_2^+ + e^- \rightarrow 1.120 \times 10^{-18} + O + O$	$3.830 \times 10^{-9} T^{-1.51}$
24	$O + O_2^+ + 2.570 \times 10^{-19} \rightarrow O^+ + O_2$	$1.890 \times 10^{-16} T^{-0.52} \exp(-18760/T)$
25	$O^+ + O_2 \rightarrow 2.570 \times 10^{-19} + O + O_2^+$	$1.890 \times 10^{-16} T^{-0.52}$
26	$N^+ + N_2 + 1.670 \times 10^{-19} \rightarrow N + N_2^+$	$1.670 \times 10^{-17} T^{-0.18} \exp(-12100/T)$
27	$O + NO^+ + 7.040 \times 10^{-19} \rightarrow O^+ + NO$	$4.580 \times 10^{-17} T^{0.01} \exp(-51000/T)$
28	$N + N + 9.340 \times 10^{-19} \rightarrow N_2^+ + e^-$	$2.980 \times 10^{-20} T^{0.77} \exp(-67650/T)$
29	$N + e^- + 2.330 \times 10^{-18} \rightarrow N^+ + 2e^-$	$1.000 \times 10^{-14} \exp(-168800/T)$
30	$O^+ + NO \rightarrow 7.040 \times 10^{-19} + O + NO^+$	$1.970 \times 10^{-17} T^{0.01}$
31	$O^+ + N_2 + 3.060 \times 10^{-19} \rightarrow O + N_2^+$	$1.055 \times 10^{-16} T^{-0.21} \exp(-22160/T)$
32	$N_2^+ + e^- \rightarrow 9.340 \times 10^{-19} + N + N$	$8.880 \times 10^{-10} T^{-1.23}$
33	$NO^+ + e^- \rightarrow 4.420 \times 10^{-19} + N + O$	$4.030 \times 10^{-9} T^{-1.63}$
34	$N_2^+ + N \rightarrow 1.660 \times 10^{-19} + N^+ + N_2$	$2.370 \times 10^{-18} T^{-0.52}$
35	$N_2^+ + O \rightarrow 3.150 \times 10^{-19} + O^+ + N_2$	$1.770 \times 10^{-17} T^{-0.21}$
36	$N + NO^+ + 8.430 \times 10^{-19} \rightarrow N^+ + NO$	$1.840 \times 10^{-15} T^{-0.02} \exp(-61060/T)$
37	$N^+ + NO \rightarrow 8.430 \times 10^{-19} + N + NO^+$	$1.840 \times 10^{-15} T^{-0.02}$
38	$O_2 + NO^+ + 4.470 \times 10^{-19} \rightarrow NO + O_2^+$	$1.720 \times 10^{-14} T^{-0.17} \exp(-32400/T)$
39	$NO + O_2^+ \rightarrow 4.470 \times 10^{-19} + NO^+ O_2$	$4.470 \times 10^{-15} T^{-0.17}$
40	$N + NO^+ + 4.900 \times 10^{-19} \rightarrow O + N_2^+$	$2.830 \times 10^{-17} T^{0.4} \exp(-35500/T)$
41	$O + N_2^+ \rightarrow 4.900 \times 10^{-19} + N + NO^+$	$4.100 \times 10^{-18} T^{0.4}$

2.4 Thermal Radiation

In a high energy, partially ionized gas, the emission of radiation is associated with changes in the electron energy. Changes in the energy of the free electrons result in free-free radiation. Bound-free radiation is produced when a photon is emitted during the recombination of an electron and ion. Bound-bound radiation occurs as a result of radiative transitions between two quantized energy levels of atoms and molecules. It is generally agreed that bound-bound transitions between the electronic states dominate under the conditions of interest. Because of the large number of radiative states and because a significant amount of the radiation comes from minor species and sparsely populated states, the radiation modeling is handled with a phenomenological modeling technique. This allows the use of a practical number of simulated molecules without experiencing the unacceptable statistical scatter which would result if each molecule were assigned a specific excited state and each excitation reaction were modeled directly.

The phenomenological model is analogous to the Borgnakke-Larsen model that is used for the rotational and vibrational degrees of freedom. There is no change to the procedures for most collisions but, for a specified fraction of collisions, the electronic states are sampled from the equilibrium distribution appropriate to the effective temperature of the molecules in the collision. This effective temperature is based on the sum of the relative translational energy and the electronic energy of the molecules. The excitation collision number is related to the ratio of the cross-section

for electronic state excitation to the elastic cross-section. Separate collision numbers are specified for the collisions of each species with neutrals, ions, and electrons. The collision numbers Bird used were based on a knowledge of the orders of magnitude of the excitation and collision cross-sections. These numbers were optimized to agree with the available radiation data for the appropriate conditions. An alternate method for determining these collision numbers is discussed in a later section.

Unlike the procedures for the rotational and vibrational energy, in which each molecule is assigned a single state, each excited particle is assigned a distribution over all the available electronic states. The sampled energy, $\bar{\epsilon}_e$, can be written as an average over the electronic states considered.

$$\bar{\epsilon}_e = (\sum \epsilon_j N_j) / N, \quad N = \sum N_j \quad (2.13)$$

Here ϵ_j is the energy of electronic level j and N_j is the number of particles in that level. From this it is concluded that a successful event excites molecules in accordance with a distribution resulting from Equation 2.13. Therefore,

$$N_j / N = \frac{g_j \exp(-\epsilon_j / kT)}{\sum g_j \exp(-\epsilon_j / kT)} \quad (2.14)$$

and g_j is the degeneracy of level j . The sum is taken over all energies of electronic states below the dissociation or ionization energy.

The molecular band system is the same as that employed by Park[9] and involves the electronic states of molecular oxygen, neutral and ionized nitrogen, and nitric oxide. These states are listed in Tables 2.3, 2.4, 2.5, and 2.6. The molecular band

transitions considered and the mean time to spontaneous emission are listed in Table 2.7. The actual time to emission in the simulation is assumed to be exponentially distributed about this mean time. One restriction in modeling radiation is that the collision routine time step must be less than the minimum radiative lifetime. As can be seen from Table 2.7, some of the lifetimes are quite small. Thus, when radiation is included a smaller simulation time step may be required and longer calculation times result.

Table 2.3. Electronic states for O_2

State	e_j (J)	g_j
1 ($X^3\sigma$)	0.	3
2 ($a^1\Delta$)	1.573×10^{-19}	2
3 ($b^1\sigma$)	2.621×10^{-19}	1
4 ($A^3\sigma$)	7.169×10^{-19}	3
5 ($B^3\sigma$)	9.891×10^{-19}	3

The states for atomic radiation have been combined to form a manageable number of groups. The groups for atomic oxygen and nitrogen are listed in Tables 2.8 and 2.9, respectively. The radiative transitions are also grouped and are referred to by number rather than spectroscopic code. Because of the grouping, each transition generally involves only a fraction of the states in the upper group. This fraction, ϕ , is included in the tables of radiative transitions. These tables are Tables 2.10 and 2.11 for atomic

Table 2.4. Electronic states for N_2

State	e_j (J)	g_j
1 ($X^1\sigma$)	0.	1
2 ($a^3\sigma$)	9.971×10^{-19}	3
3 ($B^3\pi$)	1.184×10^{-18}	6
4 ($a^1\pi$)	1.376×10^{-18}	6
5 ($C^3\pi$)	1.771×10^{-18}	2

oxygen and nitrogen, respectively.

For most of the calculations, the gas is essentially transparent to the radiation. Nevertheless, a simple physical model has been used for the calculations to estimate the probable effects of absorption in the flow. If the number density of absorbing molecules is n_a in a cell of width Δx , the probability of absorption of a photon moving at an angle of inclination θ to the axis in that cell is

$$\Delta x n_a \sigma_a / \cos \theta . \quad (2.15)$$

Here, σ_a is the absorption cross-section. In this simple model, σ_a is assumed to be constant. Each time a radiation event occurs, the angle θ is chosen such that all directions are equally possible and the trajectory of the photon is followed until it is absorbed in the flow, hits the surface, or exits from the flow. For the present calculations, the energy from the absorbed radiation is not put back into the flow. The effect of neglecting this energy will be small because the gas is optically thin.

Table 2.5. Electronic states for N_2^+

State	e_j (J)	g_j
1 ($X^2\sigma$)	0.	2
2 ($A^2\pi$)	1.791×10^{-19}	2
3 ($B^2\sigma$)	5.077×10^{-19}	2
4 ($D^2\pi$)	1.026×10^{-18}	2

Table 2.6. Electronic states for NO

State	e_j (J)	g_j
1 ($X^2\pi$)	0.	4
2 ($a^2\sigma$)	8.732×10^{-19}	2
3 ($B^2\pi$)	9.122×10^{-19}	4
4 ($C, D^2\sigma$)	1.045×10^{-18}	4
5 ($E^2\sigma$)	1.204×10^{-18}	2

Table 2.7. Molecular band system

Band	States	τ (s)	Wavelength (μ)
$N_2, 1+$	$3 \rightarrow 2$	1.1×10^{-5}	1.06
$N_2, 2+$	$5 \rightarrow 3$	2.7×10^{-8}	0.34
$O_2, S - R$	$5 \rightarrow 1$	8.2×10^{-9}	0.2
NO, β	$3 \rightarrow 1$	6.7×10^{-7}	0.22
NO, γ	$2 \rightarrow 1$	1.16×10^{-7}	0.23
$N_2^+, 1-$	$3 \rightarrow 1$	6.7×10^{-8}	0.39

Table 2.8. Groups of electronic states for O

Group	e_j (J)	g_j
1	0.	9
2	3.16×10^{-19}	5
3	6.71×10^{-19}	1
4	1.49×10^{-18}	8
5	1.73×10^{-18}	24
6	1.93×10^{-18}	72
7	2.04×10^{-18}	128
8	2.09×10^{-18}	848

Table 2.9. Groups of states for N

Group	e_j (J)	g_j
1	0.	4
2	3.82×10^{-19}	10
3	5.73×10^{-19}	6
4	1.688×10^{-18}	18
5	1.907×10^{-18}	54
6	2.073×10^{-18}	108
7	2.127×10^{-18}	54
8	2.214×10^{-18}	1314

Table 2.10. Radiative transitions for O

Number	Transition	ϕ	τ (s)	Wavelength (μ)
1	$5 \rightarrow 4$	0.6	3.3×10^{-8}	0.83
2	$6 \rightarrow 1$	0.1	2.5×10^{-8}	0.103
3	$6 \rightarrow 4$	0.01	$2. \times 10^{-6}$	0.45
4	$6 \rightarrow 5$	0.7	2.5×10^{-8}	0.99
5	$7 \rightarrow 1$	0.1	0.4×10^{-8}	0.099
6	$7 \rightarrow 5$	0.4	$1. \times 10^{-7}$	0.64
7	$8 \rightarrow 5$	0.1	$5. \times 10^{-7}$	0.55

Table 2.11. Radiative transitions for N

Number	Transition	ϕ	τ (s)	Wavelength (μ)
1	$4 \rightarrow 1$	0.5	0.5×10^{-8}	0.117
2	$4 \rightarrow 2$	0.25	0.2×10^{-8}	0.152
3	$4 \rightarrow 3$	0.25	0.5×10^{-8}	0.178
4	$5 \rightarrow 2$	0.15	0.2×10^{-8}	0.129
5	$5 \rightarrow 4$	0.08	$6. \times 10^{-8}$	0.907
6	$6 \rightarrow 2$	0.1	$1. \times 10^{-8}$	0.117
7	$6 \rightarrow 3$	0.1	$1. \times 10^{-8}$	0.132
8	$6 \rightarrow 5$	0.7	$5. \times 10^{-8}$	1.19
9	$7 \rightarrow 4$	0.1	$1. \times 10^{-6}$	0.45
10	$8 \rightarrow 2$	0.005	$3. \times 10^{-8}$	0.108
11	$8 \rightarrow 3$	0.003	$5. \times 10^{-8}$	0.121
12	$8 \rightarrow 4$	0.008	2.5×10^{-7}	0.38
13	$8 \rightarrow 5$	0.04	$1. \times 10^{-7}$	0.65

3 THE TEST CASE

The test case which has been used in the current study is a 10 km/s shock wave in air at .1 Torr. This case is used because it represents the conditions of a shock tube experiment performed at AVCO and reported by Allen, Rose and Camm in 1962[4]. The calculations are strictly one-dimensional using a 1-D standing shock wave DSMC code.

3.1 The AVCO Experiment

Photometric measurements of the radiation behind a normal air shock wave were made in an electric arc-driven shock tube at the AVCO-Everett Research Laboratory. Measurements were made of the radiation from a normal air shock at .1 Torr and 10 km/s. The report includes oscillograms that indicate the pulse shape of the global radiation from the wave at wavelengths above .24 microns, together with derived data on absolute intensity versus wavelength. The latter data are presented for radiation emitted from near the peak of the pulse and for radiation from the region of near constant radiation downstream of the peak. The two sets of measurements are referred to as ‘nonequilibrium’ and ‘equilibrium’ radiation, respectively.

The report gives the equilibrium temperature behind the shock as 9650 ± 250 K and the level of ionization as $10\% \pm 2\%$. While this degree of ionization probably represents a Saha equilibrium calculation of air properties at this temperature and pressure, the specific method used to obtain the value is not stated in the report.

In comparison, the equilibrium air properties compiled in Vincenti and Kruger[10] indicate a much lower percent ionization at similar conditions. Also, calculations made for equilibrium air using the program AIRNEW[11] give the level of ionization for these equilibrium conditions as less than 5 %.

3.2 The 1-D DSMC Code

The calculations were performed with a one-dimensional stagnation streamline code. This code is easily adapted to calculate flows with normal shocks. Initially, the code models the case of constant area flow with undisturbed freestream molecules entering at one end and a solid surface at the other end. In time, an unsteady shock wave propagates from the wall. When the shock reaches a predetermined position, molecules are removed from the downstream section of the flow such that the exit flux equals the inlet flux and the shock position remains constant. The molecule removal is conducted in such a way that mass, momentum and energy are conserved. It was shown by Bird[6] that this is achieved if the molecules are removed with a probability proportional to the square of their velocity component normal to the stream. For normal shock wave flows, the molecular removal is immediately adjacent to the wall. Thus, the remainder of the flow is exactly one-dimensional.

The simulation uses 400 cells and nearly 50,000 molecules in a region of approximately 3 cm in length. Results are the averages of the flow properties for many thousands of samples (typically 25,000 to 50,000). The calculations were performed primarily on Sun 3 and Sun 4 workstations. For convenience in displaying the results,

a shock center is defined as the point at which the density is 6 times the free stream density. This is defined as $x = 0$ in the plots. Molecules travel from $-x$ to $+x$ on average in the flow.

4 MODELING OF PLASMAS

A plasma is defined as weakly ionized when the effects of electron - neutral collisions in the flow are more important than the effects of electron - ion collisions. Similarly, a strongly ionized gas is one in which electron - ion collisions dominate. For a weakly ionized gas, it is sufficient to consider binary collisions in a solution process. The simultaneous interaction of a charged particle with all other charged particles in the Debye sphere is significant when the gas is strongly ionized. Only weakly ionized gases are presently investigated with DSMC because the programs assume binary collisions dominate. For the hypersonic reentry flows of interest in this study, multi-body charged particle collisions may be ignored if the ionization is less than 3-4 %. Although the equilibrium ionization level in the 1962 test case[4] was reported to be 10 %, more recent calculations of the chemistry in similar flows indicate that the ionization for a shock flow in air of this energy would be much less. In fact, the DSMC calculations predict an ionization level in the shock region of 2-3 %, which is well within the slightly ionized limit.

Some of the problems involved with the introduction of charged particles into DSMC procedures result from the significantly higher velocities and collision frequency of the electrons relative to the heavy particles in the flow. The collision frequency for the electrons is approximately two orders of magnitude greater than for the heavy particles. Thus, a simulation time step based on electron collision fre-

quency would be very small relative to the time step based on heavy particle collision frequency and the question of which time step is appropriate to the simulation is introduced.

Another difficulty is the question of charge neutrality in the flow. The physical requirement for charge neutrality is that an electron and ion should remain separated by less than a Debye length. This distance, ξ , is given by

$$\xi = (kT_e\epsilon/(n_e e^2))^{1/2} \quad (4.1)$$

where k is the Boltzmann constant, T_e is the electron temperature, ϵ is the permittivity of free space, e is the electronic charge, and n_e is the electron number density. This distance is typically much smaller than the molecular mean free path in the flows under consideration. Since the cell size is on the order of the mean free path, the Debye length is also much smaller than the cell size. This complicates the question of how to computationally enforce charge neutrality.

Charged particles are a minor species in the flow. This presents a further difficulty in obtaining meaningful solutions because the DSMC method depends on statistical sampling. The number of particles in the simulation and the sampling time must both be very large if one is to obtain meaningful results concerning minor species. Additionally, because each simulated molecule represents an extremely large number of real molecules, the flow fluctuations in the simulation may be many orders of magnitude larger than those in the real gas. In a charged gas this could lead to electric fields which would generally be far stronger than the real fields.

4.1 The Method of Bird

The method adopted by Bird in previous simulations represents a simple solution to some of these problems. This method was successful in demonstrating that the DSMC formalism could handle problems involving plasmas and produce reasonable solutions for the flowfields[6]. However, some of the assumptions may cause errors in the electron temperature and electron density gradient which are unacceptable for certain applications.

The procedure adopted involves associating each electron with an ion and moving the two always as a pair. Collisions and velocity components are calculated for electrons as for the heavy particles, but the electrons are moved only in relation to the movement of their associated ion. This enforces charge neutrality and allows the use of the large, heavy particle-based time step without allowing the electrons to move too far during that time step.

Because the movement of the electrons relative to the ions is restricted, the explicit evaluation of the electric field in the code is not required. However, a method for including electric field effects is incorporated because these effects may be strong at high altitudes for reentry vehicles[12, 13]. A form of the Langmuir and Tonks[14] equation

$$E = (kT_e/e) \frac{d \ln(n_e)}{dx} \quad (4.2)$$

is applied to a converged solution to obtain a value for the electric field, E . This value is then used in the simulation and a new solution obtained. The process is repeated

until the successive solutions agree within some convergence criteria.

A major drawback to the above scheme is that it depends on the spatial derivative of the electron number density. Small statistical deviations in the number density of electrons in adjacent cells can lead to large errors in the derivative. An extremely large number of samples must be taken in order to obtain a distribution which is smooth enough to provide an adequate derivative. This, combined with the iterative nature of incorporating electric field effects makes the time required to obtain a solution large. Also, when radiation in the flow is considered, the time step in the collision routine must be smaller than the shortest radiative lifetime of the transitions being considered. This time is on the order of the time step based on the electron collision frequency. Therefore, the advantage of being able to use the heavy particle based time step is removed.

Another problem with the above method is that the position of the electrons is artificially constrained (each electron associated with a specific ion). In the real flow, electrons from the higher temperature regions will diffuse into the lower temperature regions and vice versa. The use of the Langmuir and Tonks equation is questionable because it is a continuum formulation. The derivation of this equation requires the following assumptions; slightly ionized gas, net current of zero, and constant electron temperature. If the electron temperature is not constant, then E is proportional to the gradient of electron pressure and not to the gradient of electron density. Thus, the equation is not valid in the shock region.

4.2 The Ambipolar Diffusion Method

The concept of ambipolar diffusion can be used explicitly in the DSMC framework for the calculation of charged particle motion and electric field. Ambipolar diffusion results when the lighter electrons tend to diffuse out of the flow faster than the ions for flows involving a mass density gradient. A charge separation and resulting electric field are produced. The electric field retards the electron diffusion while enhancing the diffusion of the positive ions. A scheme for using this concept to determine a local electric field throughout the flowfield is outlined below.

The electric field calculations are performed in the domain of a supercell, which consists of several adjacent computational cells (typically about 10). If the net ion current is set equal to the net electron current in a given supercell, an electric field, \vec{E} , for that cell may be calculated. The calculation involves the summation over the number of charged particles in the supercell. Therefore, to minimize statistical scatter and obtain a reasonable sample of charged particles, there should be several hundred particles in a supercell. To further reduce statistical scatter, the electric field is time averaged before it is applied to the calculation of charged particle motion. Because of the disparity between the collision frequencies of the electrons and the heavy particles, each is moved based on its own time step. This yields $\Delta t_e \ll \Delta t_h$ and electrons move more often than the heavy particles. The electric field, \vec{E} , is calculated after each electron movement. The result is smoothed over the heavy particle time step, Δt_h , and used for the next Δt_h in the calculations of charged particle velocity. Even

the above smoothing technique may not solve all the problems related to statistical variations in the calculated electric field. Therefore, once the flow has reached steady state, the electric field is calculated by averaging over all the samples. This smooths out any remaining scatter in the solution.

Charge neutrality must be enforced in the simulation because the Debye length is much smaller than any other characteristic length. In the present approach, the electrons and ions are not tied together and charge neutrality is not automatically ensured. The following procedure is used if, after the movement routine is exercised, the charge neutrality condition is not satisfied. Randomly selected electrons in supercells with excess electrons are moved to randomly chosen locations in neighboring supercells which have a deficiency of electrons until the number of electrons and ions in each supercell is equal.

Details of the electric field computation are given in Appendix A. The method has the advantage of including all the flow gradients in the solution process. It is completely consistent with the statistical nature of DSMC and does not rely on a continuum equation as does the method of Bird. The diffusion properties of the high speed electrons are accounted for and their high collision frequency relative to the heavy particles is considered. One drawback to the method is that statistical scatter in the calculated electric field must be kept to a minimum. This requires large numbers of simulated molecules, small time steps, and long computational times. However, when radiation is considered in solution, the time steps for the two methods are

approximately equal and the time penalty associated with the ambipolar diffusion method is only that of the larger number of particles required in the simulation. The charge neutrality condition is not maintained over the Debye length, which is the physical requirement. However, it is maintained over the length of a supercell, which is small with respect to physical flow gradients. Therefore, this is not considered to be a problem.

4.3 Results

Results are presented for the 10 km/s standing shock wave in air at .1 Torr. The 1-D normal shock wave program was used for both sets of results, the only difference being the plasma modeling technique. In the plots, the flow is from left to right with zero at the approximate shock center. For these conditions, the flowfield composition through the shock and the translational temperature profile are given in Figures 4.1 and 4.2. The differences in the solution between the two methods would not be easily distinguishable on plots of this scale, but are detailed in the remaining figures.

The ambipolar diffusion method for the plasma calculations has a significant effect on the electron temperature through the shock, as can be seen in Figure 4.3. The peak temperature is lower and occurs further upstream of the shock. Also, energetic electrons are present through a much larger portion of the flow. The sharp peak in electron temperature which is predicted when Bird's method is used is the result of limiting the electron mobility by moving charged particles only in pairs. The broader distribution of energetic electrons seems more physically reasonable. The shift in the

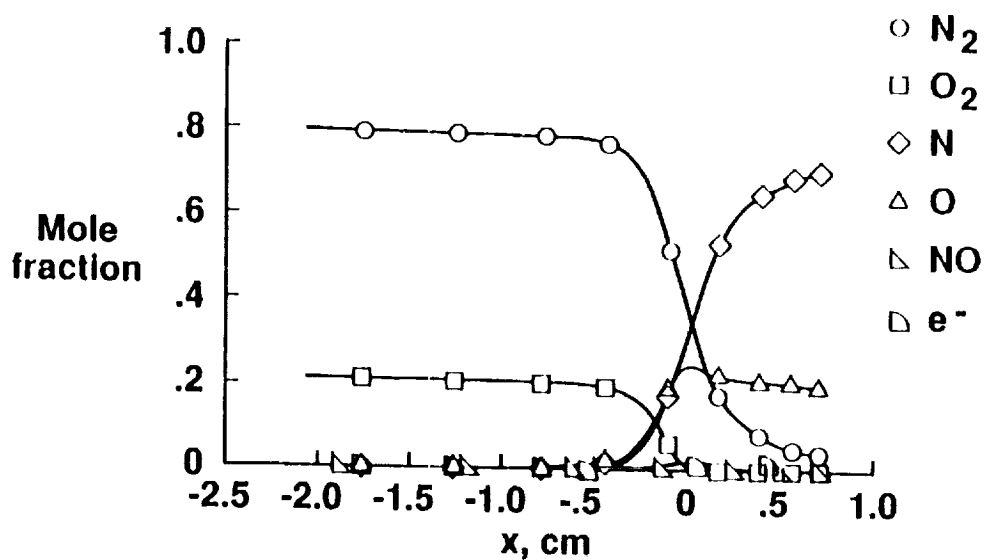


Figure 4.1. Composition through the shock

peak temperature demonstrates the tendency of the energetic electrons to diffuse to the lower density portions of the flow.

The electric field for the two cases is shown in Figure 4.4. The ambipolar diffusion method predicts a much higher electric field in the shock region. This is because this method implicitly incorporates all the flow gradients and nonequilibrium effects while the Equation 4.2 accounts only for the electron density gradient and is a continuum equation.

There is little difference in the level of ionization between the two methods (Figure 4.5) although the peak electron concentration is less with the ambipolar diffusion method. The difference is probably due to the effect of the lower electron temperature on the electron impact reactions. Both methods give an ionization level of under 3 %.

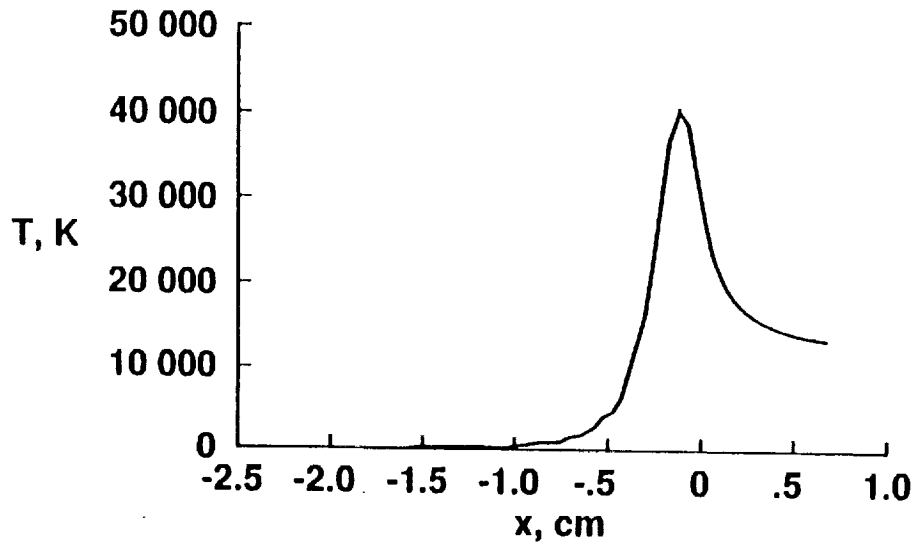


Figure 4.2. Translational temperature through the shock

This value is somewhat under the equilibrium value estimated from the AVCO data. Further comparisons with data and other computational techniques are required to determine if the level of ionization is being predicted adequately.

The radiation predicted through the shock is not greatly different for the two electric field methods (Figure 4.6). The ambipolar diffusion method results indicate about 50 % as much radiation in the equilibrium region behind the shock and approximately the same level of peak radiation. The electron temperature and gradient of electron temperature in the flow are the prime drivers for the amount of radiation predicted. Some other methods for nonequilibrium radiation, such as Park's NEQAIR[15], ignore gradients in the electron temperature and are very sensitive to the value of electron temperature used. The DSMC method always includes the effect

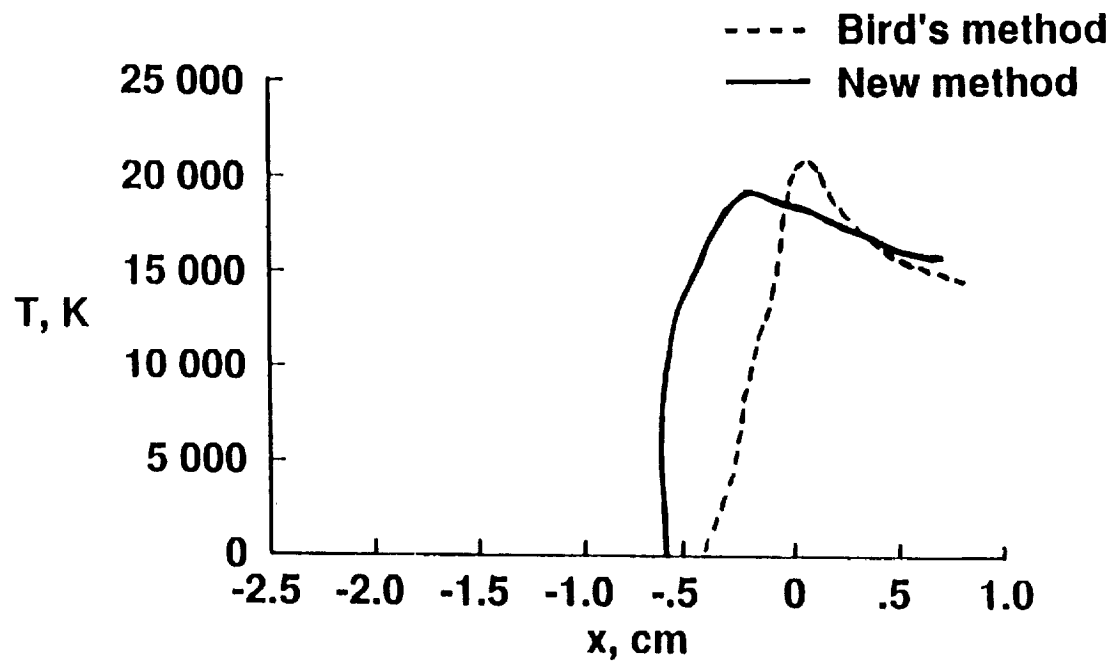


Figure 4.3. Electron temperature through the shock

of the flow gradients. It appears that the different shape of the electron temperature curve, as evidenced by the two methods, does not have as much effect on the radiation solution as neglecting the gradients entirely.

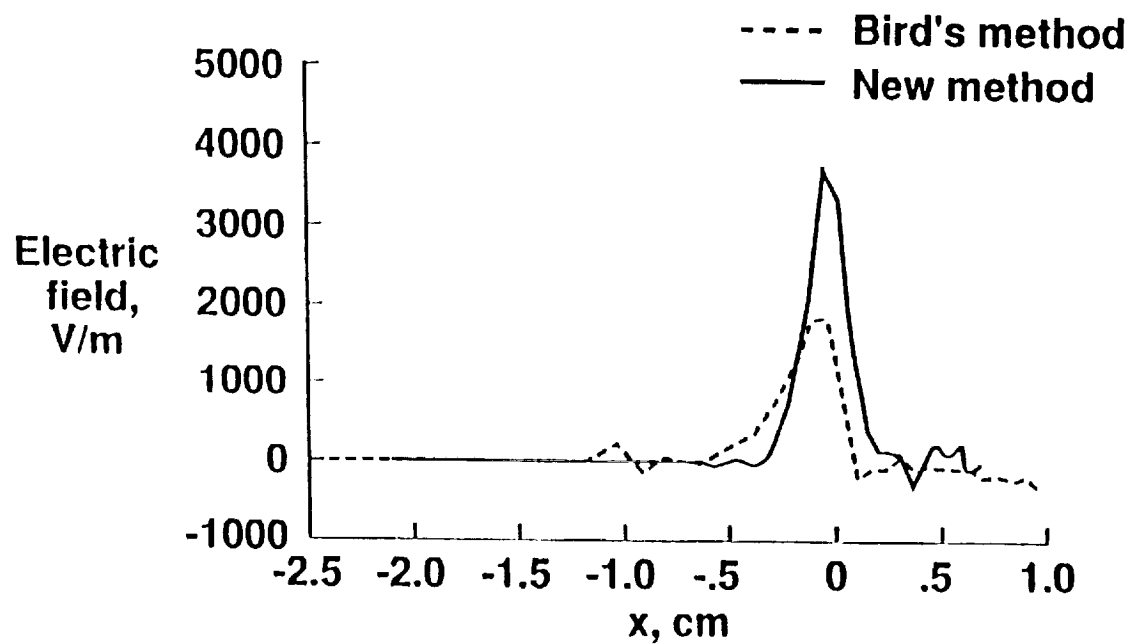


Figure 4.4. Electric field through the shock

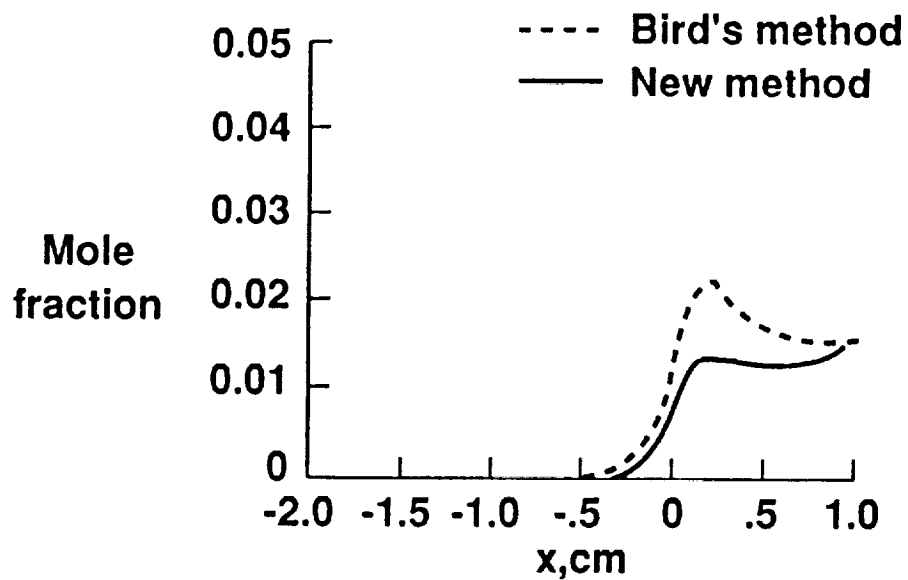


Figure 4.5. Electron concentration through the shock

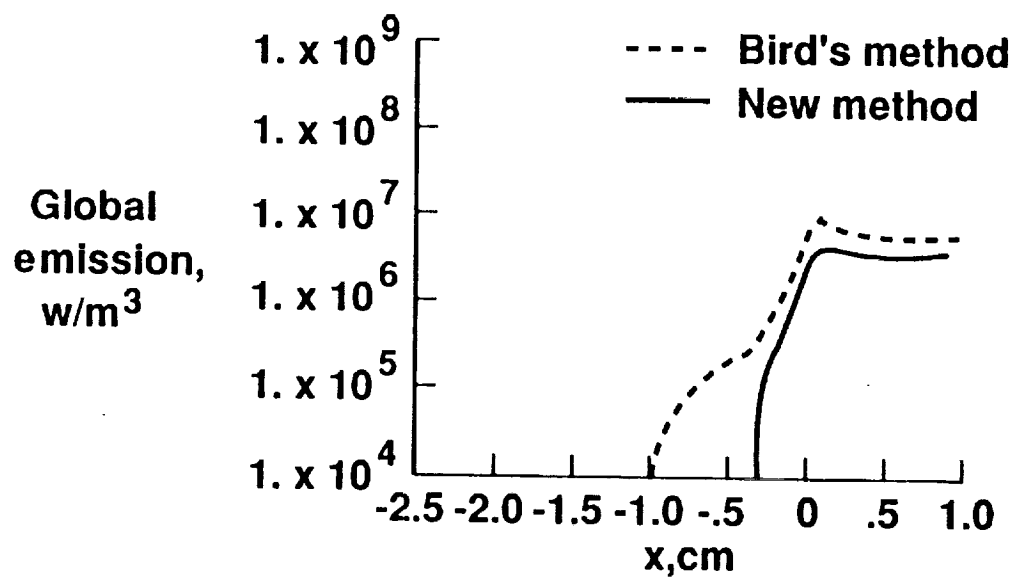


Figure 4.6. Global radiation through the shock

5 ELECTRON IMPACT IONIZATION

The flow fields considered in this study are sufficiently energetic that a significant contribution to the total ionization is from electron impact ionization reactions. The reactions have traditionally been thought of as single step reactions, but the available rate coefficients for these reactions have highly negative temperature exponents which have long been thought to be nonphysical. These rate coefficients cannot be incorporated directly into the DSMC steric factor formulation. However, the assumption that the reactions proceed via two steps has gained acceptance in recent studies. The DSMC framework makes incorporating two step reactions a straightforward task.

5.1 One Step Method

The available rate constants for the electron impact reactions are not of a form which can be used directly by the DSMC programs. The rate coefficient, $k(T)$, for a chemical reaction is specified by

$$k(T) = aT^b \exp(-E_a/(kT)) \quad (5.1)$$

where a and b are constants, E_a is the activation energy and k is the Boltzmann constant. Because of the absence of cross-section data, these rate coefficients are used to determine collisional energy dependent steric factors. The steric factor, P_r , is the ratio of the reaction cross-section to the total cross-section that results in the

above rate coefficient. It is proportional to

$$P_r \propto (1 - E_a/E_c)^{\zeta+b+1/2}, \quad E_c \geq E_a \quad (5.2)$$

where ζ is a measure of the vibrational and rotational internal degrees of freedom which may contribute to the reaction and E_c is the collisional energy. With P_r equal to zero for $E_c \leq E_a$, the representation is valid as long as

$$\zeta + b + 1/2 > 0 \quad . \quad (5.3)$$

The values of b given by Park and Menees[8] for the electron impact ionization reactions



and



are -3.9 and -3.82 respectively. Because the reactants are monatomic gases, $\zeta = 0$ and the criterion indicated by Eqn (5.3) is violated.

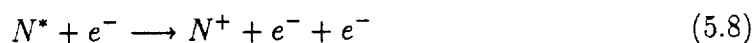
The method that has been employed to produce acceptable rates for a one step reaction involves determining an average flow temperature and replacing T^b in the rate coefficient by its value at that temperature. This, in effect, changes $k(T)$ to

$$k(T) = A \exp(-E_a/(kT)), \quad A = a(T_{avg})^b \quad . \quad (5.6)$$

This is not accurate in the immediate vicinity of the shock because the temperature is changing rapidly and is considerably different from the average temperature used in the rate calculation.

5.2 The Two Step Method

A method has been proposed which uses the assumption that these two reactions proceed via a two step chain involving excitation followed by ionization from the excited state. Thus, the ionization of atomic nitrogen proceeds by



with similar reactions for atomic oxygen. In his paper on ionization in air behind high speed shock waves, Wilson[16] asserts that the rate limiting step in this ionization process is the excitation of nitrogen atoms to the $3s^4P$ state and oxygen atoms to the $3s^5S$ state. Experimental reaction cross-sections are available for these excitation processes from Stone and Zipf[17, 18]. These cross-sections are used directly in the program when determining the probability of excitation after a collision.

One extra factor which must be taken into account is the probability of radiation from these excited states. The $3s^4P$ state of nitrogen has a short radiative lifetime, Park[15] gives the lifetime as $.2 \times 10^{-8}$ s. The oxygen state $3s^5S$ is not considered a significant source of radiation. The available data show a much larger excitation cross-section for nitrogen than for oxygen in the temperature range of interest, yet the ionization rate data indicate that the ionization rates are not much different. This tends to support the assumption that some of the excited nitrogen radiates and returns to the ground state before it has a chance to ionize. To determine the probability that

a nitrogen atom radiates, a process similar to that used for rotational and vibrational transitions is employed. A relaxation collision number, R , is determined from the product of the radiative lifetime and the average collision frequency for nitrogen atoms at that point in the flow. The quantity $1/R$ gives the probability of transition for a single collision.

For extremely rarefied flows, the calculated value of R may be less than 1. This indicates that the radiative lifetime is less than the average time between collisions. The nitrogen atom has very little chance of ionizing from the excited state in this case. Therefore, this reaction is bypassed if the relaxation collision number is less than 1. The one step reaction rate for the same flow conditions is very small, indicating that both methods predict an insignificant contribution to the total ionization from this reaction under these conditions.

For ionization from the highly excited state of either oxygen or nitrogen, the quantum defect method discussed by Griem[19] and the experimentally determined cross-section equation of Lotz[20] are used. For a single electron in the subshell and an impact electron energy near threshold, Lotz gives the reaction cross-section, σ_r as

$$\sigma_r = \frac{a(E/P_1 - 1)(1 - b)}{P_1^2} \quad (5.9)$$

where E is the electron energy and P_1 is the energy of the excited state. The values for the constants a and b in the equation are determined in accordance with the assumption that the excited states are almost hydrogenic ($a = 4. \times 10^{-14}$ cm/sec, $b = .6$). This is valid for all highly excited states of atoms. A correction to Equation 5.9 is

dictated by the quantum defect method. The formula must be multiplied by the factor n^4 where n is the effective principal quantum number.

$$n = \left(\frac{Ry}{E_\infty - P_1} \right)^{1/2} \quad (5.10)$$

Ry is the Rydberg constant and E_∞ is the ionization energy. Thus,

$$\sigma_r = \frac{n^4 a (E/P_1 - 1)(1 - b)}{P_1^2} \quad (5.11)$$

5.3 Results

Implementing the two step electron impact reaction model for the test case of a 10 km/s shock in air at .1 Torr has relatively little effect on the flow solution. Charged particles are a minor species and electron impact ionization is only one of the mechanisms for producing charged particles. However, certain differences can be seen. The two step model predicts a slightly lower electron temperature ahead of the shock (Figure 5.1) and a more level electron concentration behind the shock (Figure 5.2).

The important advantage of using the two step method is that all of the available information about the ionization process is used in the solution technique. The approximations which were required with the one step method to make the rates compatible with the DSMC steric factor formulation are eliminated. Thus, the programs can be used with a higher level of confidence in various flow regimes.

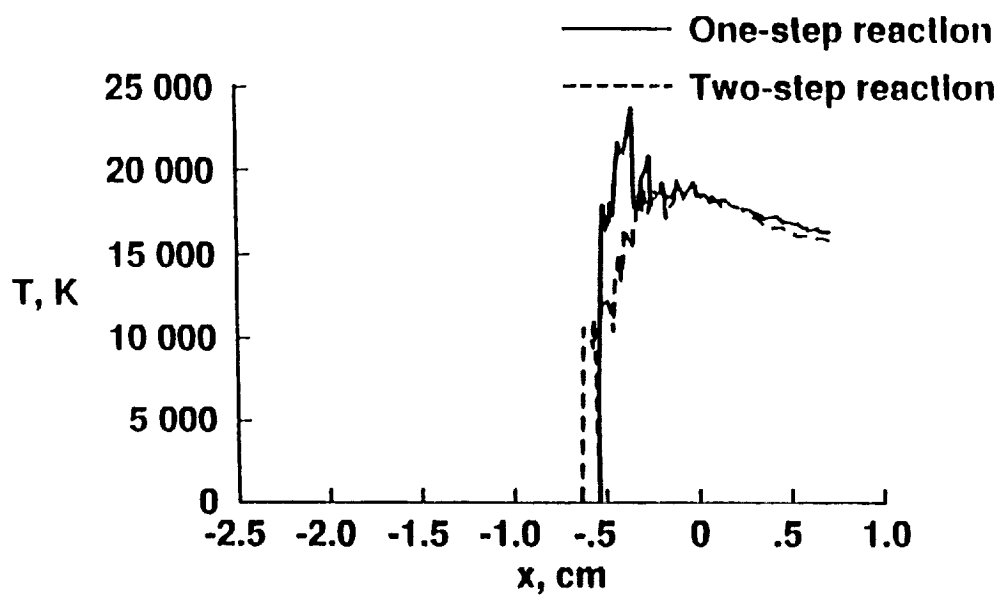


Figure 5.1. Electron temperature through the shock

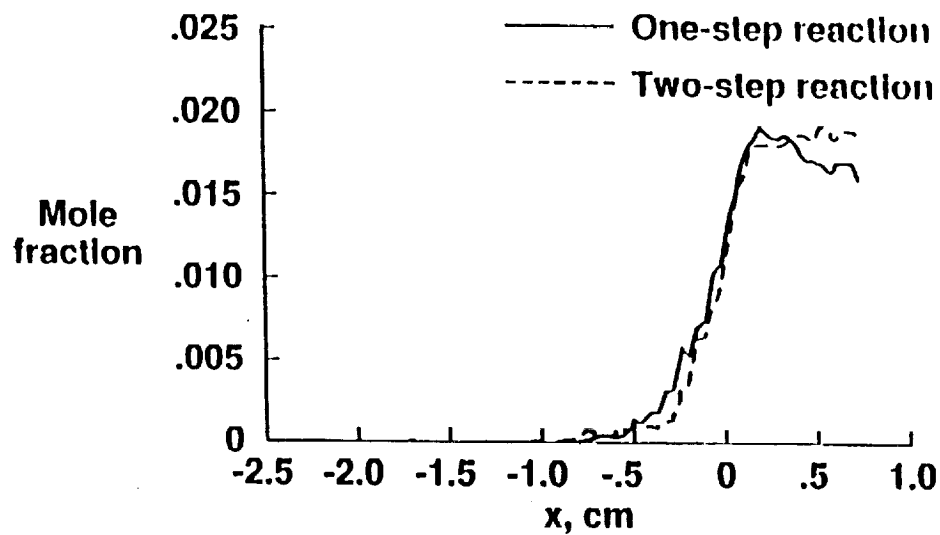


Figure 5.2. Electron concentration through the shock

6 RADIATION CALCULATIONS

In a shock wave with partial ionization, there is also electronic excitation and accompanying thermal radiation. The radiation from bound-bound transitions between electronic states is known to be significant in the 10 km/s flow of the test case. A phenomenological model is used for electronic excitation which is similar to the Borgnakke-Larsen model used in rotational and vibrational excitation. There is no change in the computation procedures for most collisions but, for a specified fraction of the collisions, the electronic states are sampled from the equilibrium distribution appropriate to the effective temperature based on the sum of the relative translational energy and the electronic energy of the molecules in the collision. In the case of electronic excitation, the molecule is assigned a distribution of states appropriate to the energy of the collision rather than a single excited state. The determination of the relaxation collision numbers for collisions of each species with electrons, ions and neutrals is the subject of this part of the study.

6.1 The Qualitative Approach

There is not much available data on the excitation cross-sections of the species involved in a real air model. Therefore, the determination of the ratio of collision cross-section to excitation cross-section, which yields the collision number, is not an easy task. Separate collisions numbers are needed for collisions of each species with neutrals, ions, and electrons. A primarily qualitative method was adopted by Bird

to demonstrate the capability of DSMC to predict nonequilibrium radiation. This method is outlined below.

The electron-ion and electron-neutral elastic cross-sections are of the order of 10^{-15} cm^2 and the data that are available for the electron impact excitation cross-sections are of the order of 10^{-16} cm^2 . This would suggest a relaxation collision number of about 10. Bird argued that, because a successful event was assumed to yield a distribution of states instead of a single state, a reduction in the cross-sections (or an increase in the collision number) was necessary. Table 6.1 shows the relaxation collision numbers which he used for electron and ion impact reactions. The values are increased by a factor of 10 for collisions with neutrals.

Table 6.1. Relaxation collision numbers for electronic excitation

Species	Number
O_2	100
N_2	100
O	500
N	1000
NO	100
N_2^+	100

The approximate nature of the numbers employed in this table detracts from their use in future radiation calculations. Also, if the correct relaxation numbers are used

for the model, compensation for replacing a level by a distribution should not be required.

6.2 The Proposed Method

The object of this part of the investigation was to provide a method to calculate the relaxation numbers which is based on the existing data and does not introduce empiricism into the procedure. This can be accomplished by using the following procedure which depends on the excitation rate data.

The reactions that are responsible for radiation are



and



where B is the species in question, M is a neutral, ion or electron, j and k are specific electronic states and $h\nu$ represents an emitted photon. The largest rates in these reactions are for collisions with charged particles. However, for a slightly ionized gas, neutral particle collisions are also important. The production rate of N_j is given by

$$dN_j/dt = [\sum_k K_M(k, j)N_k]N_M - [\sum_k K_M(j, k)]N_jN_M + [\sum_k A(k, j)N_k] - [\sum_k A(j, k)]N_j \quad (6.3)$$

where the K_M are excitation rate coefficients and the A are transition probabilities.

Multiplying by the energy of level j , ϵ_j , and summing

$$Nd\bar{\epsilon}_e/dt = d/dt(\sum \epsilon_j N_j) =$$

$$N_M \sum \epsilon_j [\] - N_M \sum \epsilon_j N_j [\] + \sum \epsilon_j [\] - \sum \epsilon_j N_j [\] \equiv N(\bar{\epsilon}_{eq} - \bar{\epsilon}_e)/\tau . \quad (6.4)$$

Here τ is a mean lifetime of the excited states. Thus, an estimate of $1/\tau$ is given by

$$1/\tau = \frac{\sum \epsilon_j N_j (K_M(j) N_M + A(j))}{\sum \epsilon_j N_j} \quad (6.5)$$

when

$$K_M(j) = \sum_k K_M(j, k) , \quad A(j) = \sum_k A(j, k) . \quad (6.6)$$

The fraction of collisions which lead to excitation is then equal to $1/\tau\nu$ where ν is the collision frequency. The needed rates are available from Parks's NEQAIR with the exception of those for molecular oxygen and the highest excited level of molecular nitrogen. Those rates were taken from Slinker and Ali[21].

The values of collision numbers obtained in the above manner are order of 1 and higher in all cases except excitation of N_2^+ . In this case the value was much less than 1, indicating more collisional excitation than collisions - a clearly unphysical process. The problem may be a result of some N_2^+ being formed in the excited state in chemical reactions, a process not accounted for in this study. It could also be a result of the uncertainties in the data or in the approximations inherent in determining the relaxation collision numbers. While this requires further study, for the current application the collision number for N_2^+ is set to 1. The collision numbers obtained for the test case after equilibrium was reached are given in Table 6.2.

Table 6.2. Relaxation collision numbers for electronic excitation

Species	Number
O_2	51
N_2	4
O	1
N	1
NO	13
N_2^+	1

The cross-sections for the collisions of neutral heavy particles are smaller, approximately by the ratio of the two masses, than those of electron collisions[9]. Therefore, the numbers for the collision fractions are reduced by this amount for neutral particles. Further details of these calculations and the rate data which were used are given in Appendix B.

The Borgnakke-Larsen approach which is used for the partitioning of electronic energy is also the approach used for the partitioning of the rotational and vibrational internal energy. This consistency of approach for the partitioning of internal energy is one of the advantages of the DSMC method of modeling nonequilibrium flows. The approach depends on the correct calculation of relaxation numbers for determining the percentage of collisions which result in the redistribution of internal energy. If these relaxation numbers are determined correctly, then it will not matter whether

the energy is assigned to a specific internal state, as with rotation and vibration, or to a distribution of states, as with electronic excitation. Since radiation is determined by the electronic energy, then as long as the average, $\bar{\epsilon}$, is computed correctly, the electronic energy of the system will remain the same whether it is assigned to one molecule or a distribution of molecules. As a result, when a large sample is considered, the results should be independent of the manner in which $\bar{\epsilon}$ is assigned. Thus, it is not necessary to alter the relaxation numbers to account for assuming a distribution of states, as was done in Bird's qualitative radiation approach.

6.3 Results

The radiation results were calculated with the 1-D standing shock wave program using the ambipolar diffusion plasma method and the two-step electron-impact ionization procedure. Both global radiation values and the spectral distribution are investigated. The effect of the radiation modeling on the translational and electron temperature predictions is also presented. The computational predictions are compared with the experimental results from the AVCO shock tube experiment[4].

The global radiation results (Figure 6.1) show large differences between the two collision excitation number methods. When Bird's qualitative method is used the intensity of radiation near the center of the shock is much lower. The new method predicts similar radiation levels in the equilibrium region behind the shock, but much larger levels in the nonequilibrium region.

The general radiation pulse shape from the oscillogram trace during the AVCO

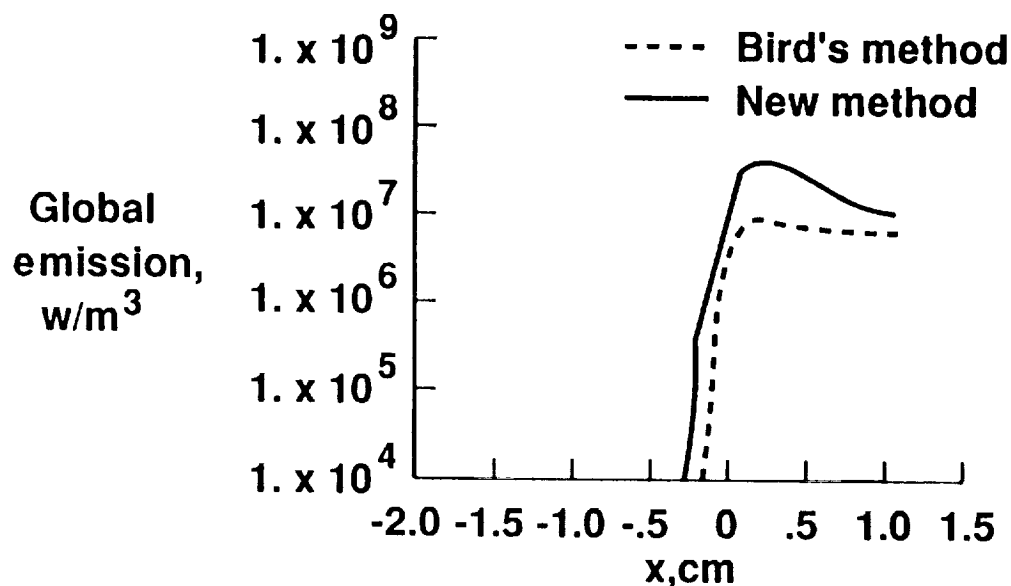


Figure 6.1. Global radiation through shock

experiment is pictured in Figure 6.2. The calculated emission is plotted against distance but, since the wave moves 1 cm in one microsecond, the comparison with the trace is easily made. The intensity scale of the trace was not calibrated, so absolute comparisons cannot be made. However, the peak nonequilibrium intensity appears to be about one order of magnitude greater than the equilibrium intensity. While both sets of data are qualitatively similar to the pulse shape, the new method data agrees better with the ratio of nonequilibrium to equilibrium intensity.

The translational temperature and electron temperature plots for the two cases are shown in Figures 6.3 and 6.4. As would be expected, both translational and electron temperature maxima are lower in the new method plots. The equilibrium temperatures behind the shock are also lower. The larger amount of radiation energy

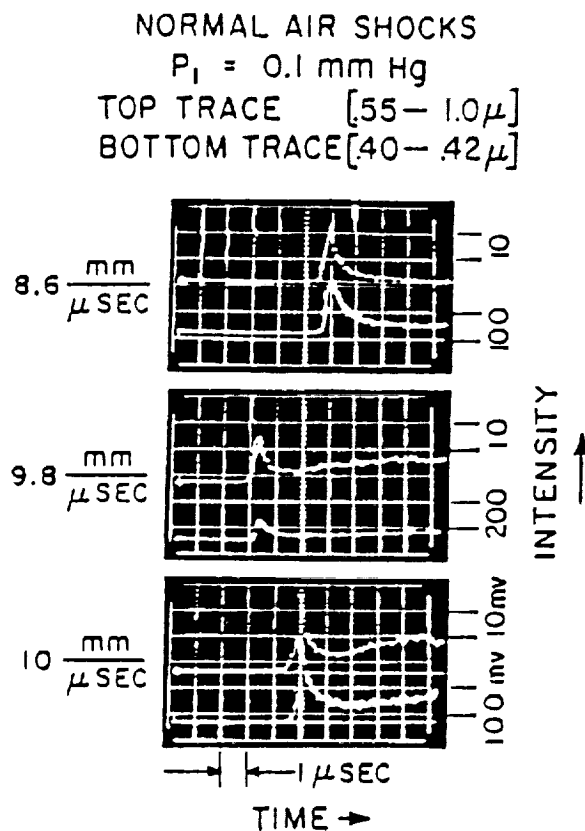


Figure 6.2. Oscillogram trace of radiation from AVCO experiment

corresponds to proportionately less energy in the other modes, hence lower temperatures. The information available from the AVCO experiment is that the equilibrium temperature was estimated to be $9650 \pm 250 \text{ K}$. The equilibrium temperature result for the new radiation method is closer to this published value.

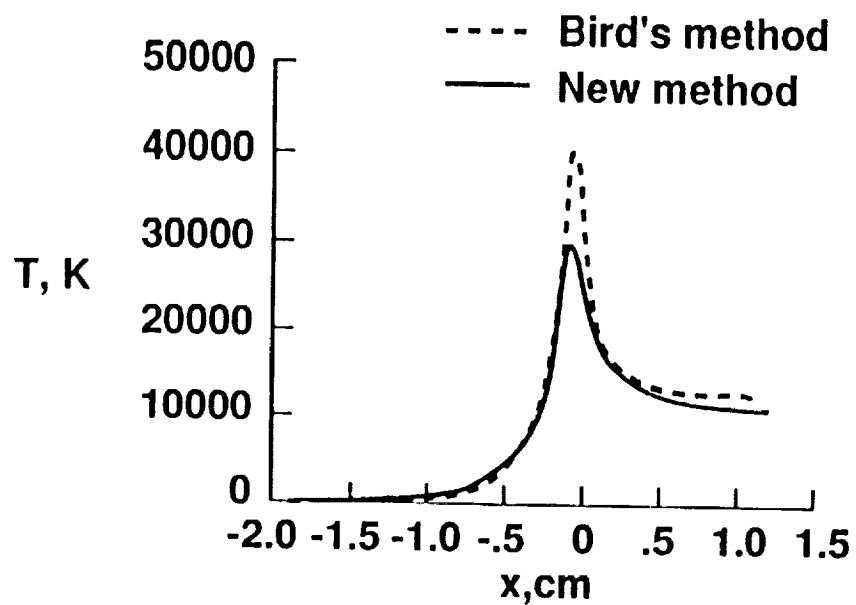


Figure 6.3. Translational temperature through the shock

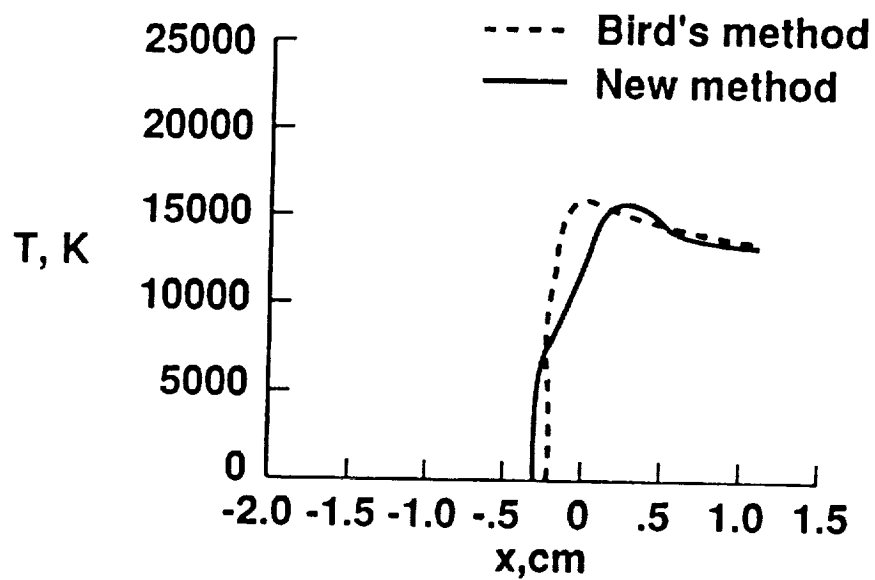


Figure 6.4. Electron temperature through the shock

6.3.1 Nonequilibrium Radiation

The experimental results for the radiation intensity versus wavelength in the nonequilibrium region are compared in Figures 6.5 and 6.6 with the results from the two DSMC runs. The radiant energy per unit volume from each of the transitions listed in Tables 2.7, 2.10, and 2.11 was spread evenly over the wavelength range defined by the midpoints between this transition and the two neighboring transitions. Then a smooth curve was drawn through these points. The new method has better qualitative agreement with the experimental data except for the overshoot of radiation at .39 microns. This overshoot is a result of the large amount of radiation from the $N_2^+, 1-$ state. As mentioned before, the radiation calculations for this ion require further work. A detailed comparison of the radiation from separate species is given in Figures 6.7, 6.8 and 6.9. The largest increase in the molecular contribution is the contribution from N_2^+ . In the region below .2 microns the new method shows a large increase in the contribution from N and O atoms. Unfortunately, no data exist to compare with the computations in this region.

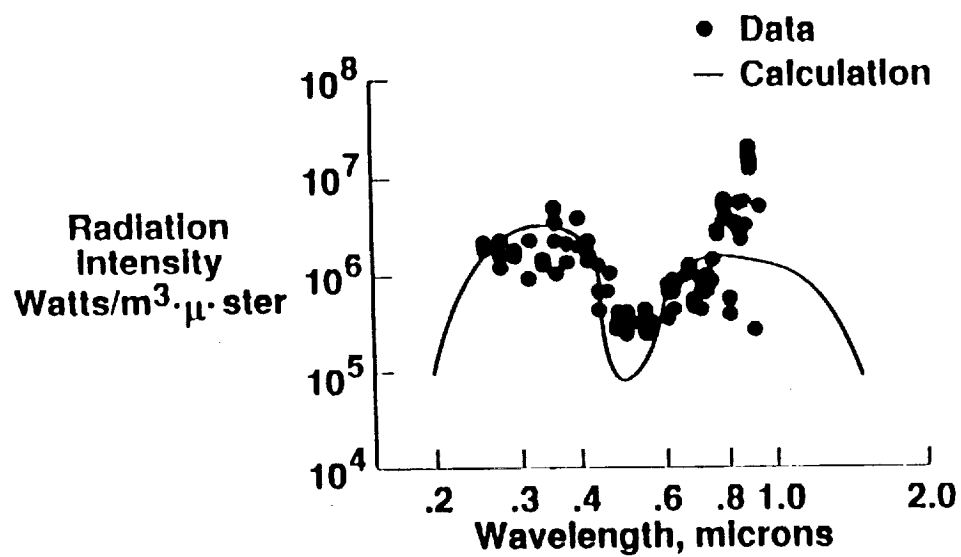


Figure 6.5. Radiation intensity vs. wavelength, Bird's method

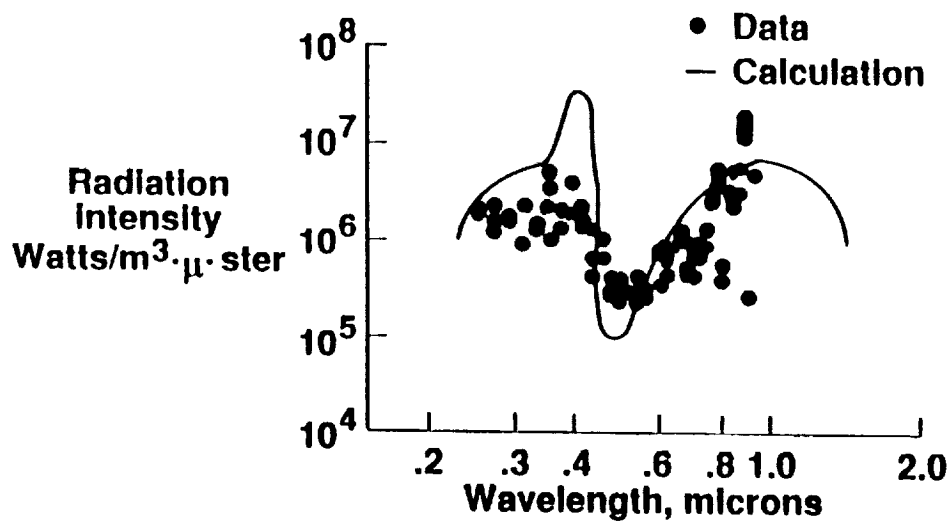


Figure 6.6. Radiation intensity vs. wavelength, new method

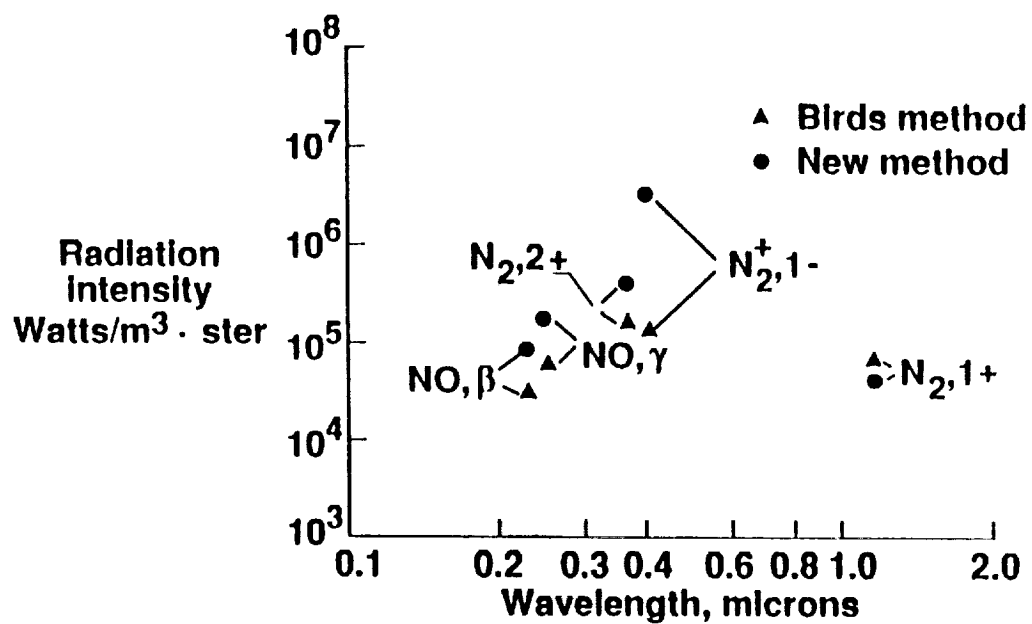


Figure 6.7. Molecular contributions to total radiation

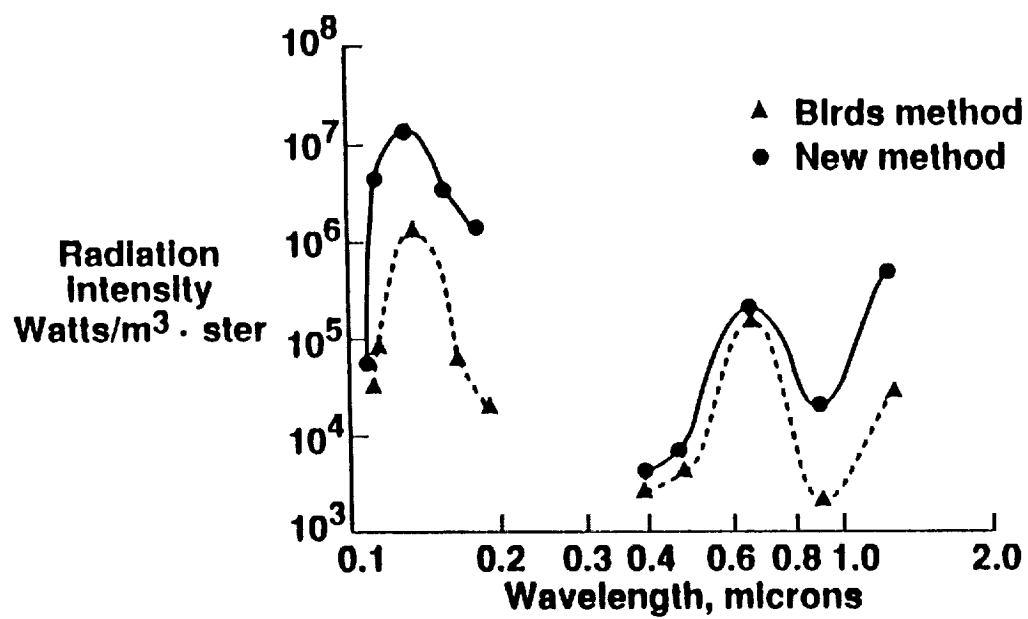


Figure 6.8. Contribution of atomic nitrogen to total radiation

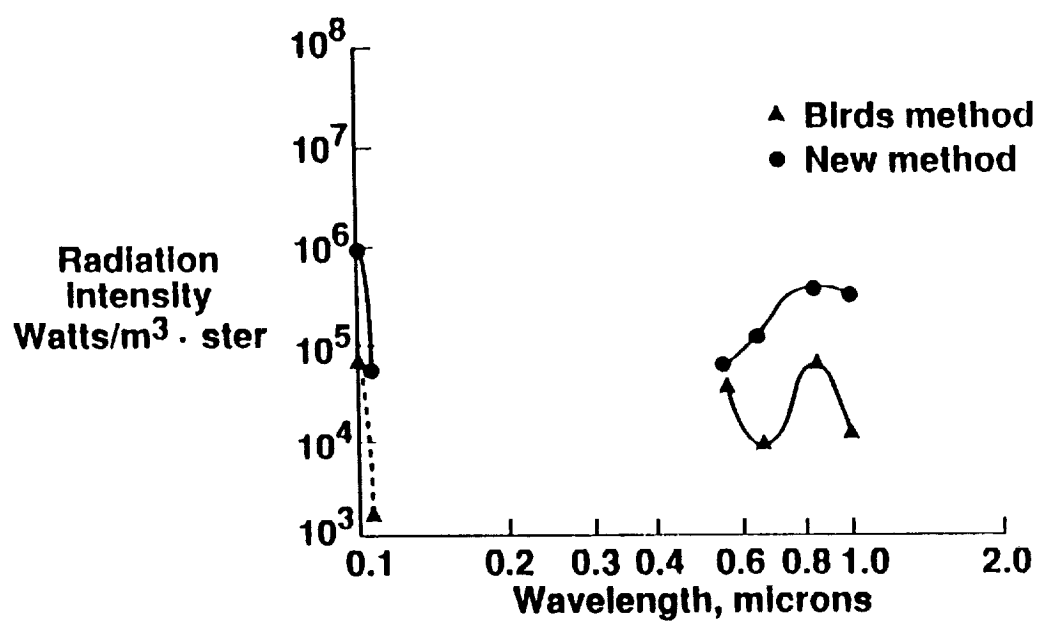


Figure 6.9. Contribution of atomic oxygen to total radiation

6.3.2 Equilibrium Radiation

The spectral distribution of radiation from the equilibrium region behind the shock is compared to the ACVO data for the two computations in Figures 6.10 and 6.11. The qualitative agreement of the data with the predictions is good except where the new method overpredicts the contribution at .39 microns, again from the $N_2^+, 1-$ transition. Detailed plots of the contributions from the molecular and atomic species are given in Figures 6.12, 6.13 and 6.14.

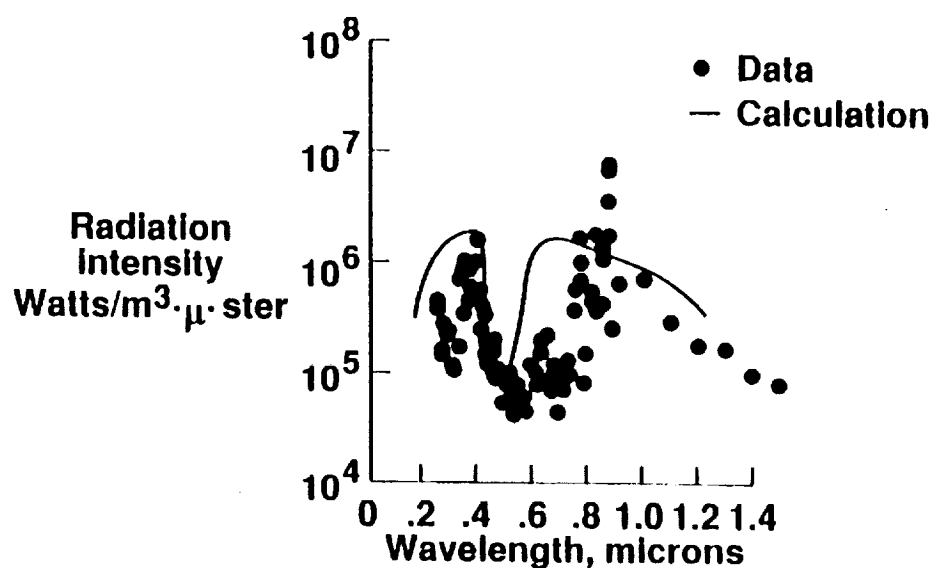


Figure 6.10. Radiation intensity vs. wavelength, Bird's method

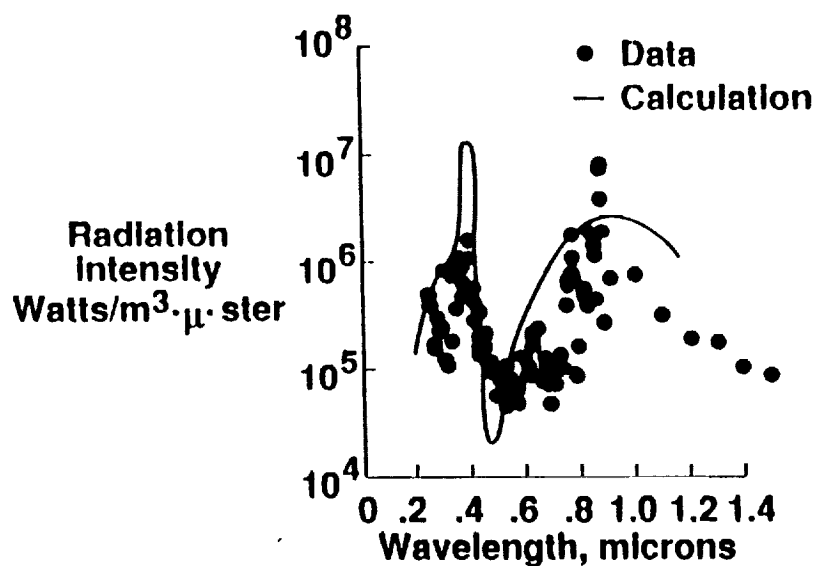


Figure 6.11. Radiation intensity vs. wavelength, new method

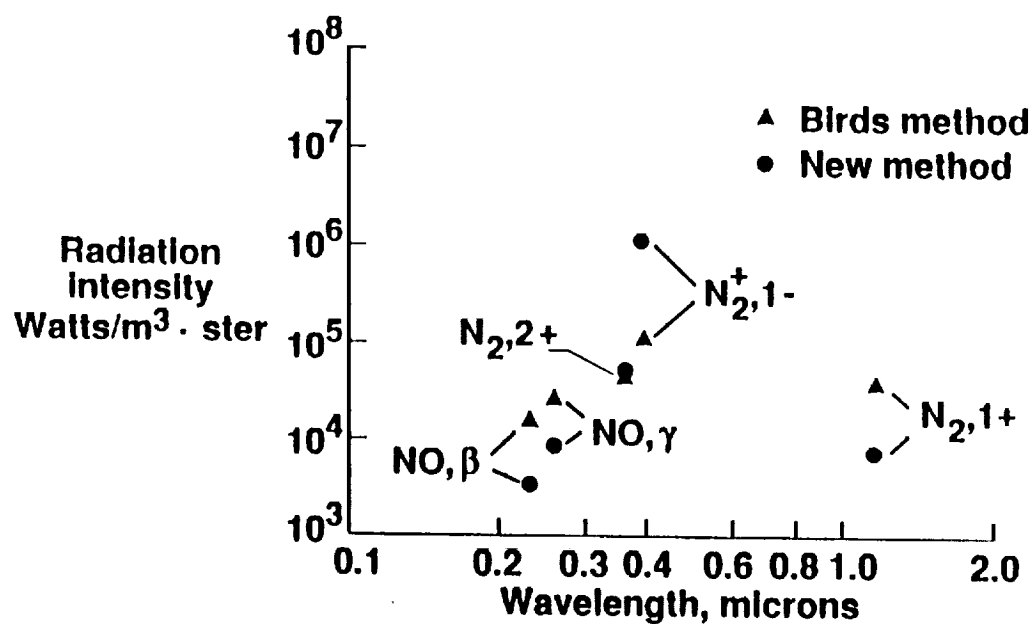


Figure 6.12. Molecular contributions to total radiation

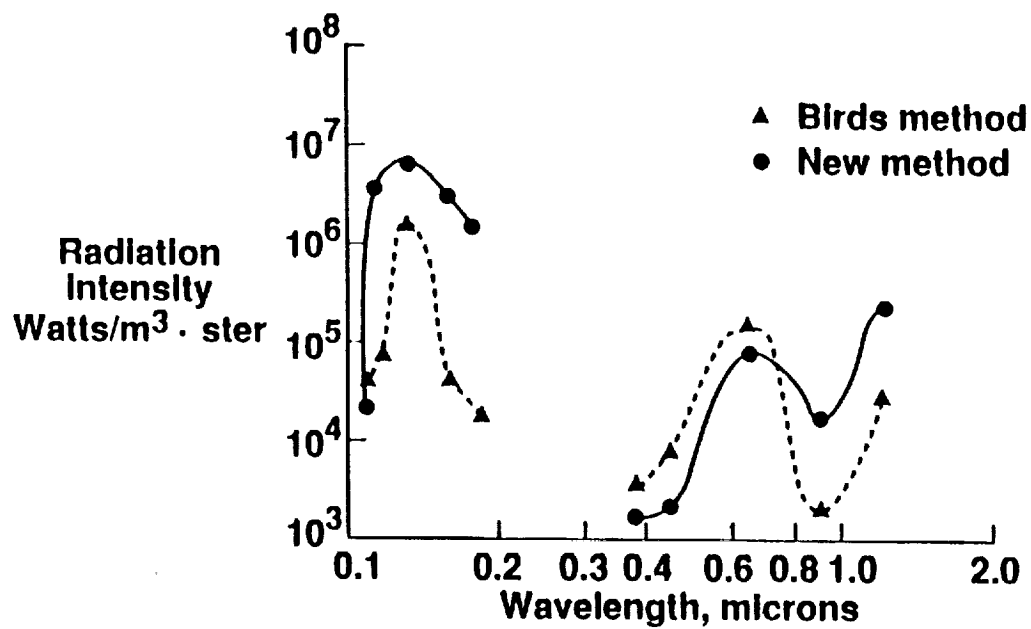


Figure 6.13. Contribution of atomic nitrogen to total radiation

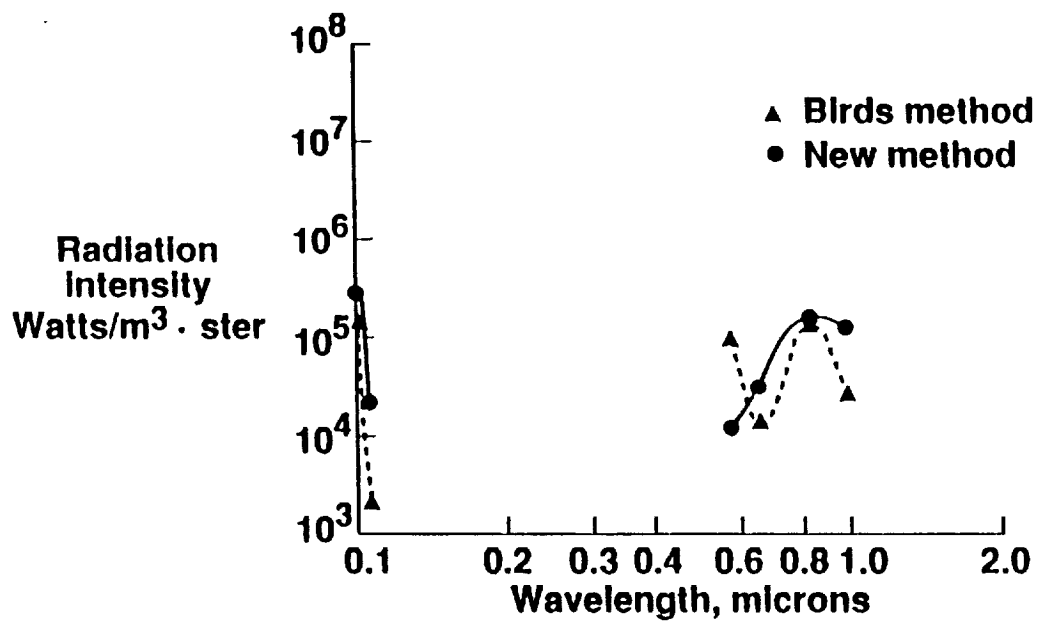


Figure 6.14. Contribution of atomic oxygen to total radiation

7 CONCLUDING REMARKS

In an effort to improve the modeling of nonequilibrium radiation with DSMC, new methods for electric field effects, electron impact ionization reactions and determining relaxation collision numbers for electronic excitation have been proposed. Results for the new models are compared with results obtained using versions of DSMC programs currently available at NASA-Langley Research Center. These results are also compared, where possible, to data from an AVCO-Everett shock tube experiment.

The new method for computing the electric field and its effect on the flow involves the assumption of ambipolar diffusion. Applying the condition of ambipolar diffusion to the flow, namely that the net ion current is equal to the net electron current at any point in the flow, allows the calculation of a local electric field. This field is then used to determine the motion of the charged particles in the flow. This method is more physically reasonable than the method which had been used previously, which was to associate each electron with a specific ion and always move the pair together. The results show a lower peak electron temperature and diffusion of high energy electrons into more regions of the flow. Although results for electron temperature are not available from the AVCO experiment, the trend of the new results is consistent with the expected high rate of electron diffusion.

The electron impact reactions were investigated because these reactions are now generally thought to proceed in two steps. The two step rates fit the experimental

data better and are more easily adapted to DSMC than the previously implemented single step reaction rates. The solution, in this case, is not significantly affected by the choice of reaction model. However, this implementation allows more of the experimental data to be included in the modeling. Thus, the confidence level is increased for flowfields of varying temperature and density conditions.

The determination of the relaxation collision numbers for electronic excitation was previously based on a qualitative knowledge of the magnitudes of excitation cross-sections compared with collision cross-sections. The numbers required some adjustment in order to obtain good agreement with the experiment of Reference [4]. A new method was proposed which bases the determination of these numbers on the available rate data for electronic excitation and values of radiative state lifetimes. It has been shown that the relaxation collision numbers obtained with this method can be used without adjustment to provide equally good radiation estimates. With the exception of the contribution to the total radiation from the N_2^+ ion, the results obtained with the new method agree more closely with the experimental values from the AVCO shock tube experiment. Further work is suggested in this area.

The modifications presented have all been implemented in one dimensional DSMC codes. The extension of these methods to two and three dimensions should be straightforward. The methods all suffer from the lack of experimental data. These data are required to supply some of the modeling parameters. They are also needed in order to evaluate whether these methods are adequate for future DSMC applications.

However, judging from the available data, the new modeling techniques appear to be improvements over those models which are currently in use.

REFERENCES

- [1] G. A. Bird. *Molecular Gas Dynamics*. Oxford University Press, London, 1976.
- [2] G. A. Bird. Nonequilibrium Radiation During Reentry at 10 km/s. AIAA Paper 87-1543, 1987.
- [3] J. N. Moss, G. A. Bird, and V. K. Dogra. Nonequilibrium Thermal Radiation for an Aeroassist Flight Experiment Vehicle. AIAA Paper 88-0081, 1988.
- [4] R. A. Allen, P. H. Rose, and J. C. Camm. Nonequilibrium and Equilibrium Radiation at Super-Satellite Reentry Velocities. Research Report 156, AVCO-Everett Research Laboratory, Everett, Mass, 1962.
- [5] G. A. Bird. Monte-Carlo Simulation in an Engineering Context. *Progress in Astronautics and Aeronautics; Rarefied Gas Dynamics*, 74(Part 1):239 – 255, 1981.
- [6] G. A. Bird. Direct Simulation of Typical AOTV Entry Flows. AIAA Paper 86-1310, 1986.
- [7] C. Borgnakke and P. S. Larsen. Statistical Collision Model for Monte Carlo Simulation of Polyatomic Gas Mixtures. *Journal of Computational Physics*, Vol 18:405–420, 1975.

- [8] C. Park and G. P. Menees. Odd Nitrogen Production by Meteoroids. *Journal of Geophysical Research*, Vol. 83:4029 – 4035, 1978.
- [9] C. Park. Calculation of Nonequilibrium Radiation in the Flight Regimes of Aeroassisted Orbital Transfer Vehicles. *Progress in Astronautics and Aeronautics*, Vol. 96:395 – 418, 1985.
- [10] W. A. Vincenti and C. H. Kruger, Jr. *Introduction to Physical Gas Dynamics*. John Wiley and Sons, Inc., New York. London. Sydney, 1965.
- [11] R. K. Prabhu and W. D. Erickson. A Rapid Method for the Computation of Equilibrium Chemical Composition of Air to 15 000 K. NASA TP 2792, 1988.
- [12] C. J. Schexnayder, Jr., P. W. Huber, and J. S. Evans. Calculation of Electron Concentration for a Blunt Body at Orbital Speeds and Comparison With Experimental Data. NASA TN D-6294, 1971.
- [13] W. L. Jones, Jr. and A. E. Cross. Electrostatic Probe Measurements of Plasma Parameters for Two Reentry Flight Experiments at 25,000 Feet per Second. NASA TN D-6617, 1972.
- [14] I. Langmuir and I. Tonks. *Physics Reviews*, Vol. 34:874, 1929.
- [15] C. Park. Nonequilibrium Air Radiation (NEQAIR) Program: Users Manual. NASA TM 86707, 1985.

- [16] J. Wilson. Ionization Rate of Air Behind High Speed Shock Waves. *Physics of Fluids*, Vol. 9(No. 9):1913–1921, 1966.
- [17] E. J. Stone and E. C. Zipf. Excitation of Atomic Nitrogen by Electron Impact. *Journal of Chemical Physics*, Vol. 58:4278–4284, 1973.
- [18] E. J. Stone and E. C. Zipf. Electron-Impact Excitation of the 3S and 5S States of Atomic Oxygen. *Journal of Chemical Physics*, Vol. 60:4237 – 4243, 1974.
- [19] H. R. Griem. *Plasma Spectroscopy*. McGraw - Hill Book Company, New York, 1964.
- [20] C. Lotz. Electron-Impact Ionization Cross-Sections and Ionization Rate Coefficients for Atoms and Ions from Hydrogen to Calcium. *Zeitschrift für Physik*, Vol. 216:231 – 247, 1968.
- [21] S. Slinker and A. W. Ali. Electron Excitation and Ionization Rate Coefficients for N₂, O₂, NO, N and O. NRL Memorandum Report 4756, Naval Research Laboratory, 1982.

8 APPENDIX A: ELECTRIC FIELD CALCULATIONS

The details of how the ambipolar diffusion concept is used to calculate a supercell electric field are included in this appendix. Recall that a supercell is a region in the computational space which consists of several cells, enough to get a sample consisting of several dozens of charged particles. In this region, it is possible to calculate an electric field by setting the net electron current equal to the net ion current, as required by ambipolar diffusion. For a small time interval, Δt , \vec{E} may be assumed constant. The following set of equations outlines the procedure used to compute \vec{E} for this Δt .

It should be noted that these equations are written over individual particles in the simulation and the charged particle velocity, \vec{v}_s , is the instantaneous velocity of a single charged particle. With this in mind, the average velocity of a single charged particle during the time step, Δt , is given by

$$\vec{v}_s = \vec{v}_{s,0} + (q_s \vec{E} \Delta t / 2m_s) \quad (8.1)$$

where $\vec{v}_{s,0}$ is the particle velocity at the beginning of the time step, m_s is the particle mass and q_s is the particle charge. The mass average ion velocity for that time step is

$$\vec{V}_i = \frac{\sum m_\alpha \vec{v}_\alpha N_\alpha}{\sum m_\alpha N_\alpha} \quad (8.2)$$

where α refers to an ion species and N_α is the number of particles of that species in

the supercell. The average electron velocity during the time step is

$$\vec{V}_e = \sum \vec{v}_{e,0}/N_e - (e\vec{E}/m_e)(\Delta t/2) \quad (8.3)$$

where e is the charge of the electron. Because charge neutrality is required in the supercell, $N_e = \sum N_\alpha$. The electric field is calculated by setting $\vec{V}_i = \vec{V}_e$ and solving the resulting equation. The result can be written as

$$e\vec{E}\Delta t/2 = \frac{\sum \vec{v}_{e,0}/N_e - \sum m_\alpha \vec{v}_{\alpha,0} N_\alpha / \sum m_\alpha N_\alpha}{\sum N_\alpha / \sum m_\alpha N_\alpha + 1/m_e} \quad (8.4)$$

A simplification of Equation 8.4 is useful in reducing the computational time of the solution. Note that the term $1/m_e$ in the denominator is much larger than the term $\sum N_\alpha / \sum m_\alpha N_\alpha$. Thus, an approximation to Equation 8.4, good to better than .1 %, is

$$e\vec{E}\Delta t/2m_e = \sum \vec{v}_{e,0}/N_e - \sum m_\alpha \vec{v}_{\alpha,0} N_\alpha / \sum m_\alpha N_\alpha \quad (8.5)$$

Because the electric field calculation is performed each time step, it is desirable to make the computation as efficient as possible.

At first glance, it appears that the result for the electric field, a physical parameter, is dependent on the computational time step. This is not the case. The right hand side of Equation 8.5 also has a dependence on the time step through the equations for the individual particle velocities. The result for electric field has been demonstrated to be time step independent as long as the requirement that the time step be less than the local average collision time (Equation 2.1) is met.

9 APPENDIX B: RELAXATION NUMBERS

The equations given in section (6.2) for determining the electronic excitation relaxation numbers depend on values for the rate coefficient, $K(i, j)$, for collisional transitions between states i and j . They also depend on the transitional probability of a radiative state, $A(i)$, for state i . The $A(i)$ are simply the inverse of the average lifetime of the radiative state. Thus, the values for $A(i)$ can be determined directly from the values in Tables 2.7, 2.10 and 2.11. The values for $K(i, j)$ must be obtained from some other source.

The program NEQAIR[15] is a well known and generally accepted nonequilibrium radiation code. The values of $K(i, j)$ for nearly all the transitions of interest were taken from this code. Tables of $K(i, j)$ vs. temperature are stored in the computer with values of $K(i, j)$ at intervals of 5000 K. The NEQAIR output with the pertinent rates is included in the following pages (Table 9.1). The values of $K(i, j)$ for transitions to the fifth excited level of N_2 and all the values of $K(i, j)$ for O_2 transitions were obtained from Slinker and Ali[21] because they were not available in NEQAIR. These are listed in Tables 9.2 and 9.3. The backwards rates are calculated from the equilibrium condition.

$$K(j, i) = K(i, j) \frac{g_i \exp(-\epsilon_i/kT)}{g_j \exp(-\epsilon_j/kT)} \quad (9.1)$$

Table 9.1. Excitation rate coefficients from NEQAIR

```

molecular band name=N2+      molecular weight=    28.010
number of electron-impact dissociation cross-section set= 4
number of electron-impact excitation cross-section set  = 6
number of electronic levels      = 5
number of levels in quasi-steady-state calc.            = 4
  degen      term      we      wexe      weye      weze      be      alpha

molecular band name=N2      molecular weight=    28.010
number of electron-impact dissociation cross-section set= 4
number of electron-impact excitation cross-section set  = 6
number of electronic levels      = 5
number of levels in quasi-steady-state calc.            = 4
  degen      term      we      wexe      weye      weze      be      alpha

molecular band name=NO      molecular weight=    30.010
number of electron-impact dissociation cross-section set= 3
number of electron-impact excitation cross-section set  = 3
number of electronic levels      = 6
number of levels in quasi-steady-state calc.            = 3
  degen      term      we      wexe      weye      weze      be      alpha

molecular band name=O2      molecular weight=    32.000
number of electron-impact dissociation cross-section set= 0
number of electron-impact excitation cross-section set  = 0
number of electronic levels      = 5
number of levels in quasi-steady-state calc.            = 0
  degen      term      we      wexe      weye      weze      be      alpha
SPECIES:N2+
m,n      1      2
te, rate= 1000.000      0.2563332e-11
te, rate= 6000.000      0.2301418e-06
te, rate= 11000.00      0.7025959e-06
te, rate= 16000.00      0.1129382e-05
te, rate= 21000.00      0.1517553e-05
te, rate= 26000.00      0.1884031e-05
te, rate= 31000.00      0.2237865e-05
te, rate= 36000.00      0.2583836e-05
te, rate= 41000.00      0.2924625e-05
te, rate= 46000.00      0.3261837e-05
te, rate= 51000.00      0.3596479e-05
te, rate= 56000.00      0.3929218e-05
m,n      1      3
te, rate= 1000.000      0.3171157e-21
te, rate= 6000.000      0.7641024e-08
te, rate= 11000.00      0.1507309e-06
te, rate= 16000.00      0.5170711e-06
te, rate= 21000.00      0.1048720e-05
te, rate= 26000.00      0.1681843e-05
te, rate= 31000.00      0.2375036e-05
te, rate= 36000.00      0.3103867e-05
te, rate= 41000.00      0.3854053e-05
te, rate= 46000.00      0.4617129e-05
te, rate= 51000.00      0.5387981e-05
te, rate= 56000.00      0.6163458e-05
m,n      1      4
te, rate= 1000.000      0.9206178e-38
te, rate= 6000.000      0.4972897e-10
te, rate= 11000.00      0.1449090e-07
te, rate= 16000.00      0.1152792e-06
te, rate= 21000.00      0.3370318e-06
te, rate= 26000.00      0.6512300e-06

```

```

te, rate= 31000.00      0.1020321e-05
te, rate= 36000.00      0.1417343e-05
te, rate= 41000.00      0.1826205e-05
te, rate= 46000.00      0.2237713e-05
te, rate= 51000.00      0.2647045e-05
te, rate= 56000.00      0.3051821e-05
m,n      2      3
ml= 2 mu= 3 d1= 8.255e-04 d2= 2.125e-03 f1= -8.73 s1=-3.434e-17
ml= 2 mu= 3 d1= 8.233e-04 d2= 2.099e-03 f1= -5.14 s1=-7.278e-19
ml= 2 mu= 3 d1= 8.492e-04 d2= 2.073e-03 f1= -11.3 s1=-1.601e-18
ml= 2 mu= 3 d1= 8.212e-04 d2= 2.073e-03 f1= -1.66 s1=-9.136e-21
ml= 2 mu= 3 d1= 8.730e-04 d2= 2.021e-03 f1= -13.6 s1=-7.503e-20
ml= 2 mu= 3 d1= 8.449e-04 d2= 2.021e-03 f1= -4.21 s1=-9.809e-22
ml= 2 mu= 3 d1= 8.708e-04 d2= 1.996e-03 f1= -9.99 s1=-2.330e-21
ml= 2 mu= 3 d1= 8.967e-04 d2= 1.970e-03 f1= -15.6 s1=-3.650e-21
ml= 2 mu= 3 d1= 8.428e-04 d2= 1.996e-03 f1=-0.848 s1=-9.131e-24
te, rate= 1000.000      0.5898820e-16
te, rate= 6000.000      0.3133399e-07
te, rate= 11000.00      0.2659963e-06
te, rate= 16000.00      0.7000613e-06
te, rate= 21000.00      0.1259443e-05
te, rate= 26000.00      0.1892296e-05
te, rate= 31000.00      0.2568533e-05
te, rate= 36000.00      0.3271102e-05
te, rate= 41000.00      0.3990146e-05
te, rate= 46000.00      0.4719793e-05
te, rate= 51000.00      0.5456429e-05
te, rate= 56000.00      0.6197765e-05
m,n      2      4
te, rate= 1000.000      0.1572189e-32
te, rate= 6000.000      0.1032268e-09
te, rate= 11000.00      0.1070387e-07
te, rate= 16000.00      0.5828956e-07
te, rate= 21000.00      0.1399615e-06
te, rate= 26000.00      0.2393661e-06
te, rate= 31000.00      0.3446425e-06
te, rate= 36000.00      0.4495669e-06
te, rate= 41000.00      0.5513766e-06
te, rate= 46000.00      0.6490530e-06
te, rate= 51000.00      0.7424793e-06
te, rate= 56000.00      0.8318875e-06
m,n      3      4
te, rate= 1000.000      0.3460469e-23
te, rate= 6000.000      0.3519834e-08
te, rate= 11000.00      0.7607755e-07
te, rate= 16000.00      0.2335750e-06
te, rate= 21000.00      0.4275028e-06
te, rate= 26000.00      0.6345925e-06
te, rate= 31000.00      0.8467726e-06
te, rate= 36000.00      0.1061234e-05
te, rate= 41000.00      0.1276931e-05
te, rate= 46000.00      0.1493438e-05
te, rate= 51000.00      0.1710558e-05
te, rate= 56000.00      0.1928184e-05
SPECIES:N2
m,n      1      2
te, rate= 1000.000      0.8978652e-40
te, rate= 6000.000      0.2297946e-13
te, rate= 11000.00      0.6501143e-11
te, rate= 16000.00      0.5695121e-10
te, rate= 21000.00      0.1843136e-09
te, rate= 26000.00      0.3903246e-09
te, rate= 31000.00      0.6625867e-09
te, rate= 36000.00      0.9869230e-09
te, rate= 41000.00      0.1351322e-08
te, rate= 46000.00      0.1746492e-08

```

```

te, rate= 51000.00      0.2165456e-08
te, rate= 56000.00      0.2603010e-08
m,n      1      3
te, rate= 1000.000      0.5392893e-45
te, rate= 6000.000      0.6139224e-14
te, rate= 11000.00      0.4249107e-11
te, rate= 16000.00      0.5057353e-10
te, rate= 21000.00      0.1898078e-09
te, rate= 26000.00      0.4374875e-09
te, rate= 31000.00      0.7834800e-09
te, rate= 36000.00      0.1209964e-08
te, rate= 41000.00      0.1699717e-08
te, rate= 46000.00      0.2238507e-08
te, rate= 51000.00      0.2815247e-08
te, rate= 56000.00      0.3421483e-08
m,n      1      4
te, rate= 1000.000      0.2763280e-51
te, rate= 6000.000      0.3637676e-15
te, rate= 11000.00      0.7246945e-12
te, rate= 16000.00      0.1286724e-10
te, rate= 21000.00      0.5954451e-10
te, rate= 26000.00      0.1559450e-09
te, rate= 31000.00      0.3041409e-09
te, rate= 36000.00      0.4989995e-09
te, rate= 41000.00      0.7331409e-09
te, rate= 46000.00      0.9993196e-09
te, rate= 51000.00      0.1291269e-08
te, rate= 56000.00      0.1603856e-08
m,n      2      3
ml= 2 mu= 3 d1= 5.065e-04 d2= 1.840e-03 f1=-1.184e-02 s1=-6.046e-14
ml= 2 mu= 3 d1= 5.067e-04 d2= 1.814e-03 f1=-2.509e-03 s1=-1.126e-15
ml= 2 mu= 3 d1= 5.326e-04 d2= 1.788e-03 f1=-2.365e-02 s1=-1.061e-14
ml= 2 mu= 3 d1= 5.585e-04 d2= 1.762e-03 f1=-4.434e-02 s1=-1.989e-14
ml= 2 mu= 3 d1= 5.327e-04 d2= 1.762e-03 f1=-1.394e-02 s1=-5.729e-16
te, rate= 1000.000      0.4964567e-14
te, rate= 6000.000      0.8886260e-09
te, rate= 11000.00      0.4026861e-08
te, rate= 16000.00      0.8414079e-08
te, rate= 21000.00      0.1343679e-07
te, rate= 26000.00      0.1880550e-07
te, rate= 31000.00      0.2437770e-07
te, rate= 36000.00      0.3007780e-07
te, rate= 41000.00      0.3586278e-07
te, rate= 46000.00      0.4170666e-07
te, rate= 51000.00      0.4759290e-07
te, rate= 56000.00      0.5351054e-07
m,n      2      4
te, rate= 1000.000      0.5230360e-20
te, rate= 6000.000      0.8755541e-10
te, rate= 11000.00      0.9816033e-09
te, rate= 16000.00      0.2707609e-08
te, rate= 21000.00      0.4892172e-08
te, rate= 26000.00      0.7319792e-08
te, rate= 31000.00      0.9883529e-08
te, rate= 36000.00      0.1252834e-07
te, rate= 41000.00      0.1522412e-07
te, rate= 46000.00      0.1795346e-07
te, rate= 51000.00      0.2070574e-07
te, rate= 56000.00      0.2347423e-07
m,n      3      4
te, rate= 1000.000      0.4879294e-14
te, rate= 6000.000      0.1684055e-08
te, rate= 11000.00      0.7210704e-08
te, rate= 16000.00      0.1393221e-07
te, rate= 21000.00      0.2100262e-07
te, rate= 26000.00      0.2820276e-07

```

```

te, rate= 31000.00      0.3546015e-07
te, rate= 36000.00      0.4274597e-07
te, rate= 41000.00      0.5004716e-07
te, rate= 46000.00      0.5735719e-07
te, rate= 51000.00      0.6467256e-07
te, rate= 56000.00      0.7199127e-07
SPECIES:NO
m,n      1      2
te, rate= 1000.000      0.7931265e-38
te, rate= 6000.000      0.1233073e-14
te, rate= 11000.00      0.2257244e-12
te, rate= 16000.00      0.1874863e-11
te, rate= 21000.00      0.6174839e-11
te, rate= 26000.00      0.1350780e-10
te, rate= 31000.00      0.2371595e-10
te, rate= 36000.00      0.3644785e-10
te, rate= 41000.00      0.5132559e-10
te, rate= 46000.00      0.6800653e-10
te, rate= 51000.00      0.8619933e-10
te, rate= 56000.00      0.1056628e-09
m,n      1      3
te, rate= 1000.000      0.6654399e-37
te, rate= 6000.000      0.1771598e-12
te, rate= 11000.00      0.2921174e-10
te, rate= 16000.00      0.2033612e-09
te, rate= 21000.00      0.5786446e-09
te, rate= 26000.00      0.1127892e-08
te, rate= 31000.00      0.1806470e-08
te, rate= 36000.00      0.2577051e-08
te, rate= 41000.00      0.3412707e-08
te, rate= 46000.00      0.4294790e-08
te, rate= 51000.00      0.5210464e-08
te, rate= 56000.00      0.6150821e-08
m,n      2      3
te, rate= 1000.000      0.
te, rate= 6000.000      0.
te, rate= 11000.00      0.
te, rate= 16000.00      0.
te, rate= 21000.00      0.
te, rate= 26000.00      0.
te, rate= 31000.00      0.
te, rate= 36000.00      0.
te, rate= 41000.00      0.
te, rate= 46000.00      0.
te, rate= 51000.00      0.
te, rate= 56000.00      0.
SPECIES:O2

```


Table 9.2. Rate coefficients for N_2 , fifth level

Temp (K)	Rate Coefficient ($\text{m}^3/(\text{molecule s})$)
6000.	12×10^{-14}
11000.	5.1×10^{-12}
16000.	7.0×10^{-11}
21000.	2.2×10^{-10}
26000.	4.7×10^{-10}
31000.	7.3×10^{-10}
36000.	1.0×10^{-9}
41000.	1.1×10^{-9}
46000.	1.5×10^{-9}
51000.	1.6×10^{-9}
56000.	1.8×10^{-9}

Because of the time involved in calculation of the relaxation collision numbers, they are calculated only once in each 40 or 50 iterations. The average temperature of each species in the nonequilibrium region of flow is used for interpolation of the rate coefficients with temperature. From these values and the transition probabilities, new relaxation collision numbers are obtained. Once steady state is reached, the values change very little from calculation to calculation.

Table 9.3. Rate coefficients for O_2

Temp (K)	Rate Coefficient ($m^3/(molecule\ s)$)			
	1, 2	1, 3	1, 4	1, 5
6000.	7.4×10^{-11}	1.7×10^{-11}	1.6×10^{-12}	3.1×10^{-13}
11000.	2.4×10^{-10}	5.9×10^{-11}	2.5×10^{-11}	4.1×10^{-11}
16000.	4.2×10^{-10}	1.0×10^{-10}	9.3×10^{-11}	3.4×10^{-10}
21000.	5.8×10^{-10}	1.4×10^{-10}	1.9×10^{-10}	1.0×10^{-9}
26000.	7.0×10^{-10}	1.7×10^{-10}	3.2×10^{-10}	2.0×10^{-9}
31000.	7.8×10^{-10}	1.9×10^{-10}	4.4×10^{-10}	3.1×10^{-9}
36000.	8.4×10^{-10}	2.0×10^{-10}	5.6×10^{-10}	4.3×10^{-9}
41000.	8.8×10^{-10}	2.1×10^{-10}	7.0×10^{-10}	6.0×10^{-9}
46000.	9.2×10^{-10}	2.2×10^{-10}	8.1×10^{-10}	6.9×10^{-9}
51000.	9.4×10^{-10}	2.3×10^{-10}	9.0×10^{-10}	8.0×10^{-9}
56000.	9.5×10^{-10}	2.4×10^{-10}	9.7×10^{-10}	9.0×10^{-9}